Research paper

Pre-clinical study of iron oxide nanoparticles fortified artesunate for efficient targeting of malarial parasite

Deepika Kannan [a], Nisha Yadav [b], Shakeel Ahmad [c], Pragya Namdev [c], Souvik Bhattacharjee [c], Bimlesh Lochab [b],**, Shailja Singh [c],*

[a] Department of Life Sciences, School of Natural Sciences, Shiv Nadar University, Gautam Buddha Nagar, India
[b] Department of Chemistry, School of Natural Sciences, Shiv Nadar University, Gautam Buddha Nagar, India
[c] Special Center for Molecular Medicine, Jawaharlal Nehru University, New Mehrauli Road, New Delhi, India

A R T I C L E   I N F O

A B S T R A C T

Background: Artesunate the most potent antimalarial is widely used for the treatment of multidrug-resistant malaria. The antimalarial cytotoxicity of artesunate has been mainly attributed to its selective, irreversible and iron-radical-mediated damage of parasite biomolecules. In the present research, iron oxide nanoparticle fortified artesunate was tested in *P. falciparum* and in an experimental malaria mouse model for enhancement in the selectivity and toxicity of artesunate towards parasite. Artesunate was fortified with nontoxic biocompatible surface modified iron oxide nanoparticle which is specially designed and synthesized for the sustained pH-dependent release of Fe^{2+} within the parasitic food vacuole for enhanced ROS spurt.
Methods: Antimalarial efficacy of Iron oxide nanoparticle fortified artesunate was evaluated in wild type and artemisinin-resistant *Plasmodium falciparum* (R539T) grown in O + ve human blood and in *Plasmodium berghei* ANKA infected swiss albino mice. Internalization of nanoparticles, the pH-dependent release of Fe^{2+}, production of reactive oxygen species and parasite biomolecule damage by iron oxide nanoparticle fortified artesunate was studied using various biochemical, biophysical, ultra-structural and fluorescence microscopy. For determining the efficacy of ATA-IONP+ART on resistant parasite ring survival assay was performed.
Results: The nanoparticle fortified artesunate was highly efficient in the 1/8th concentration of artesunate IC_{50} and led to retarded growth of *P. falciparum* with significant damage to macromolecules mediated *via* enhanced ROS production. Similarly, preclinical *In vivo* studies also signified a radical reduction in parasitemia with ~8–10-fold reduced dosage of artesunate when fortified with iron oxide nanoparticles. Importantly, the ATA-IONP combination was efficacious against artemisinin-resistant parasites.
Interpretation: Surface coated iron-oxide nanoparticle fortified artesunate can be developed into a potent therapeutic agent towards multidrug-resistant and artemisinin-resistant malaria in humans.
Fund: This study is supported by the Centre for Study of Complex Malaria in India funded by the National Institute of Health, USA.

1. Introduction

Emergence and establishment of an infectious disease rely on evolutionarily dynamic infectious pathogens. Classified as the deadliest infectious disease, malaria accounts for nearly 5% of the reported death with an estimate of nearly 219 million cases of malaria occurring worldwide in 2017 [1,2]. Global burden of malaria is prevalent in tropical regions such as sub-Saharan African countries and South East Asian countries, where *Plasmodium falciparum* and *Plasmodium vivax* accounts for 99% of the estimated cases. *P. falciparum*, the predominant parasite in the South-East Asian region accounts for 62.8% cases while *P. vivax* accounts for 37.2% of all estimated cases [2]. The disease involves a complex life cycle of the *Plasmodium* with multiple stages in their vertebrate host and mosquito vector. Being clinically relevant majority of the disease associated symptoms are prevalent in the blood stage of the parasite life cycle. Currently, various drugs targeting the blood stage includes Artemisinin, Chloroquine, Tri-oxanes, Pyronaridine, *etc.*

The Chinese herb, a sesquiterpene lactone-based drug, artemisinin is at present the most potent drug against malaria certified by WHO.

* Correspondence to: S. Singh, Department of Life Science, Shiv Nadar University, NH91, Tehsil Dadri Gautam Buddha Nagar, Uttar Pradesh 201314, India.
** Correspondence to: B. Lochab, Department of Chemistry, School of Natural sciences, Shiv Nadar University, Gautam Buddha Nagar, Uttar Pradesh 201314, India.
E-mail addresses: bimlesh.lochab@snu.edu.in (B. Lochab), shailjasingh@mail.jnu.ac.in (S. Singh).

Research in context

Evidence before this study

Artemisinin the first-line therapy against *P. falciparum* exerts its antimalarial activity by ROS production through iron-catalyzed cleavage of its endoperoxide bridge. However, the decline in the efficacy of artemisinin-based drugs due to the emergence of resistant parasites jeopardizes global efforts to control and eliminate malaria.

Added value of this study

We report that nontoxic biocompatible iron oxide nanoparticle fortification of artesunate improves its efficacy by 5–10 folds. The fortification of artesunate with ATA-IONP enhances the ROS mediated irreversible damages to biomolecules resulting in enhanced cell death in artemisinin sensitive and resistant parasites.

Implications of all the available evidence

The potential use of iron oxide nanoparticle fortified artesunate a nanomedicine therapy, for the treatment of multidrug resistance and artemisinin-resistant malaria parasites.

Artemisinin and its derivatives carry a 1,2,4-trioxane core that comprises the core activity *via* endoperoxide linkage [3]. These drugs are exceptionally capable of reducing the parasite load per cycle by 10,000-fold during asexual blood-stages [4,5]. Despite its activity, very short *in vivo* half-lives (typically ⟨1−3h⟩ in humans and frequent recrudescence of infection are the major disadvantages of the drug [(6,7)].

To overcome these limitations, WHO introduced artemisinin-based Combination Therapies (ACTs) against malaria where artemisinin derivatives are co-administered with longer half-life partner drugs, such as Lumefantrine, Amodiaquine, Piperaquine, Mefloquine, Sulphadoxine-Pyrimethamine or Pyronaridine. These combinations help substantially in preventing disease upsurge and reduces parasite growth [8,9]. Chiefly the potency of the artemisinin and effectiveness of the long shelf life counter drug determines the efficacy of the ACT to reduce or eliminate the parasite load [10]. Recent reports highlight the development of resistance by the parasite against ACTs as defined by slow parasite clearance rate (*i.e.*, long parasite clearance half-life) [11]. Slow parasite clearance results in a longer exposure of greater parasite load to ACTs. These parasite populations undergo genetic mutation such as K13 propeller mutations or gene duplication thereby gaining drug resistance rendering ACT failure [12,13]. Mutations in K13 have been reported with different sensitivities to Artemisinin and its derivatives in Cambodian and African region. Various mutations such as C580Y, R539T, I543T, Y493H have been correlated with Artemisinin resistance in the field [14]. Several efforts made for prohibiting these ACT failures include identification of genotypic and phenotypic markers of ART resistance, improving plasma half-life of artemisinin and its derivatives, use of better drug delivery system or nanocarriers improvising nanomedicine to enhance the efficacy of the combination drugs.

The chemical structure of artemisinin and its derivatives explains an endoperoxide bond mediated activity. Cleavage of the endoperoxide bond is mediated by the use of ferrous ion as a catalyst. In *Plasmodium*-infected RBCs, artemisinin and its derivatives depend on soluble heme or free labile iron pool within the cytoplasm of infected RBCs [15]. This iron dependency mediates the selectivity of artemisinin and its synthetic derivatives towards infected erythrocytes over uninfected erythrocytes. The dependency of iron by artemisinin was further investigated by Stocks et al. [16] proving the efficacy of these drugs antagonizes in combination with iron chelator Deferoxamine (DFO - selective for non-heme sources of iron). These studies suggest the prerequisite of iron for artemisinin to facilitate ROS response, covalently binding to the parasite macromolecules, eventually causing DNA lipid and protein damage. Relative to these studies we suggest the provision of free iron may augment artesunate activity within parasitized RBCs. However, the supplementation of free iron in the case of malaria patients has always been controversial in terms of lethality [17,18]. Earlier studies in malaria-endemic areas have depicted the beneficial effect of iron supplements in patients suffering from iron deficient anemia and severe malaria-associated anemia [19,20]. It was observed the effect incurred in such patients due to hematological advancements (such as hemoglobin recovery) upon iron supplements combined with antimalarials. Controversially, results from other studies indicated a failure to clear malaria in a large proportion of people. Nwanyanwu et al. [20] and Verhoef et al. [21] suggested non-anemic people suffering from malaria had adverse effects of high levels of parasitemia when supplemented iron with anti-malarial. While in another trial Sazawal et al. [22] also interpreted iron supplements may ease malarial treatment in iron-deficient individuals and may increase the risk of illness in uncomplicated malaria patients with iron sufficiency. In all these studies, iron supplements have been the source of ferrous iron (Fe^{2+}). In parasite-infected RBCs, erythrocytes and parasite cytoplasm possess iron as hemoglobin as well as labile active ferrous state iron pool. Malarial parasite metabolizes hemoglobin for nutrient source and utilizes intraerythrocytic labile pool as an iron source [23,24]. Therefore, the provision of iron supplements in the active form (Fe^{2+}) may result in increased bioavailability of active iron within the labile pool favoring rapid growth of the parasite. It's been well studied, upon pathogen interaction, human host tends to oxidize ferrous into storage form ferric (Fe^{3+}), limiting the iron source for the pathogen [25,26]. This indicates the parasite growth may be abrogated by the limited availability of Fe^{2+}. Thus, we hypothesize the use of surface coated iron oxide nanoparticle may catalyze sustained release of Fe^{2+} along with the drug artesunate to enhance its efficacy.

Based on the nanoparticle-mediated approach, nanomedicine sets a new rationale to augment the action of a drug. Nanoparticles offer large surface area enabled multiple drug loading, improved drug delivery, higher affinity to host cells *via* multivalent interaction resulting in an enhanced activity [27]. Iron oxide nanoparticles (IONPs) are one of the most important classes of inorganic nanoparticles, especially superparamagnetic Fe_3O_4 nanoparticles (magnetite core). Recently, application of a carbohydrate coated iron oxide nanoparticle - Ferumoxytol (FDA approved) as an iron supplement has been widespread for curing several diseases like chronic kidney disease, IDA and cancer [28–30]. Herein, we explored the capacity of surface coated iron oxide NPs (IONPs) to enhance the efficacy of the malarial drug artesunate. Combination of surface coated iron oxide nanoparticle with artesunate boosted the efficacy of artesunate by 8-10fold both *in vivo* and 5-fold *in vitro*. Since our iron oxide NPs have an organic coating of 2-aminoterephthalic acid (ATA), it offers the sustained release of Fe^{2+} in a pH-dependent manner. The internalization of IONPs within the parasite food vacuole, a low pH environment, provided the best combination for the slow conversion of ferric to ferrous ions enabling the sustainable release of the ferrous ions, persistent activation of artesunate and generation of radical species *via* endoperoxide cleavage. In line with this, we also observed heightened DNA damage and protein damage in our combination of treated cells. Furthermore, the surface coating of ATA-IONP has inverse toxic effects of iron both *in vivo* and *in vitro*. Finally, this study provides a strategic approach to mediate controlled drug activation, improving the half-life of the drug and might be useful against drug-resistant parasites making the drug more efficacious.

2. Materials & methods

2.1. Materials

Iron (III) chloride hexahydrate, 98%, Iron (II) Chloride Tetrahydrate, ATA (2−amino−terephthalic acid), (NH4OH, 30% in water) were

purchased from Alfa Aeser. o-Phenanthroline (Fischer scientific), 5-(and-6)-carboxy-2′,7′-dichlorodihydrofluorescein diacetate (carboxy-H2DCFDA), NHS-fluorescein-dextran (NHS-FITC), Antifade DAPI, RPMI 1640, Albumax I, LysoTracker Red DND-99 (Invitrogen: Carlsbad, CA, USA), Methanol, Ethanol, ethyl acetate (MERCK, India), L- Ascorbic acid (Vitamin C), Artesunate, hypoxanthine, Sodium bicarbonate, Sorbitol, Gentamycin, Giemsa stain, DMSO, low-melting-point agarose, normal melting point agarose, ethidium bromide, 2,4-Dinitrophenylhydrazine, Trichloroacetic acid, guanidine hydrochloride, Bovine serum albumin (Sigma Aldrich), percoll (GE, India), 3-(4,5-dimethylthiazol-2-yl)-2,5-diphenyltetrazolium bromide (Thermo Fisher Scientific), RIPA buffer (Himedia Labs, India).

All chemicals were used as received without further purification.

2.2. Methods

2.2.1. Synthesis of iron oxide nanoparticles

Reagents 300 mg of $FeCl_3 \times 6\ H_2O$, 100 mg of $FeCl_2 \times 4\ H_2O$, 200 mg of ATA (2−amino−terephthalic acid) were added to 6 mL deionized (DI) water in a round bottom flask together, heated at 80 °C for 60 min. under magnetic stirring with nitrogen gas flow directly blowing in the reaction mixture. Then 1.5 mL of NH_4OH (30% in water) was added rapidly into the solution, which resulted in the nucleation of Iron oxide nanoparticles (ATA-IONPs). The resulting suspension was kept at 80°C for another 60 min under vigorous magnetic stirring and then cooled down to room temperature. The final pH of the solution was basic. The so-formed magnetic nanoparticles were magnetically isolated, centrifuged and washed with a mixture of DI water and ethanol (10 mL, 1:1 vol/vol) several times (4 washings) to yield 127 mg of coated ATA-IONPs. Coated iron oxide nanoparticles were synthesized in a similar fashion without the use of ATA.

2.2.2. Quantitative measurement of released Fe^{2+} from iron oxide nanoparticles by the method of o-phenanthroline with different pH

$FeCl_3$ (4 mM) was diluted to different concentration and reduced to Fe^{2+} by Vitamin C (10 mM, 1 mL) for 5 min, then the mixture was reacted with o-phenanthroline (0.1%, 1 mL) and the red complex was produced, with absorbance at 512 nm. The volume of the reaction system was 5 mL. The absorption spectra of different samples were obtained using an UV–vis spectrometer. The absorbance intensity at 512 nm was correlated with the Fe^{2+} ion concentration. The obtained standard curve is y=0.00479× +0.0579 (y: absorbance value at 512 nm; x: concentration of Fe^{2+} with R^2 = 0.9703). ATA-IONPs (50 μg/mL, 300 μL) were re-suspended in phosphate buffered saline (PBS) (pH 5.0, 6.0 and 7.4) and were reacted with the system of o-phenanthroline with Vitamin C and without Vitamin C for different time (0.5 h, 3 h, 6 h, 9h, 15 h and 48 h). The absorbance was then detected with UV–vis absorption technique and the Fe^{2+} released were calculated quantitatively.

2.2.3. Characterizations

Absorbance measurements were carried out on Thermo Scientific Evolution 201 UV–visible (UV–vis.) spectrophotometer in 1 cm quartz cuvettes over the range of 200–900 nm by preparing the dispersions of nanomaterial in de-ionized water. Fourier transform infrared (FTIR) spectra were recorded on a Nicolet iS5 spectrometer equipped with iD5-ATR (Diamond) accessory, in the range of 4000 to 400 cm^{-1} with a resolution of 4 cm^{-1}. X-Ray diffraction (XRD) studies were performed on Rigaku Smart Lab X-Ray Diffractometer, CuKα radiation (λ = 1.5406 Å). Thermal behavior was investigated using Perkin Elmer Diamond STG-DTA in the temperature range 50–800 °C under a nitrogen atmosphere at a heating rate of 10°C/min. Bath sonicator (Sonics) was used for sonication of ATA-IONPs for 1 min in deionized water. Transmission electron microscope (TEM) micrographs and selected area electron diffractions (SAED) were taken on a JEOL 2100F microscope. Scanning electron microscope (SEM) micrographs and energy-dispersive

spectroscopy (EDS) were taken on a Zeiss EVO40 microscope at an accelerating voltage of 5 keV. The average particle size of the nanoparticles in different pH buffers (7.4, 6 and 5) was measured by the dynamic light scattering (DLS) instrument (Nanosizer, Malvern, UK) with an argon laser wavelength λ = 830 nm, at a detector angle = 90° at room temperature. Dried powder samples were placed on an aluminum holder with double-sided adhesive carbon tape. The average size of nanoparticles from the TEM images was determined based on the measurement of the diameter of 15 nanoparticles each at different pH using Image J software.

2.2.4. Parasite culture

2.2.4.1. Plasmodium falciparum. In vitro culture of P. falciparum laboratory strain, 3D7, artemisinin sensitive (PfKelch13^{WT}) and artemisinin resistant (PfKelch13^{R539T}) strain was maintained in RPMI 1640 supplemented with 27.2 μg/mL of hypoxanthine, 5μg/L Gentamycin and 0.5% Albumax I, using O+ RBCs (2% hematocrit) in mixed gas environment (5% O2, 5% CO2 and 90% N2) as described previously [31] and synchronized using 5% sorbitol. O+ RBCs were obtained from Rotary blood bank, Delhi.

2.2.4.2. Plasmodium berghei. Animal studies were performed in accordance with guidelines of the Institutional Animal Ethics Committee (IEAC) of Jawaharlal Nehru University (JNU), Delhi and Committee for Control and Supervision of Experiments on Animals (CPCSEA). The experiments performed and the use of laboratory animals were approved and were in strict accordance following the ethical guidelines approved by the animal ethics committee IEAC-JNU. Mice obtained from Central Laboratory Animal Resources, Jawaharlal Nehru University, Delhi were housed under standard conditions of food, temperature (25 °C ± 3), relative humidity (55 ± 10%) and illumination (12 h light/dark cycles) throughout the experiment.

P. berghei ANKA strain was procured from ATCC, India. The parasites were injected intraperitoneally (10^6 parasites in 200μL 1xPBS) in Swiss albino female mice (8–10 weeks old). We determined the parasitemia with Giemsa stained tail blood smears that were made every day. Mice devoid of parasite injection were considered as an uninfected control.

2.2.5. Preparation of the combination (iron oxide nanoparticle and artesunate)

A stock solution of nanoparticles was prepared by reconstituting in sterile water. Prior usage, nanoparticles were bath sonicated for 2 min to get them into dispersion form. The required amount of nanoparticle (w/v) was mixed with artesunate (w/v) and again bath sonicated for 2 min followed by 5–10 min incubation. Combination of artesunate with iron oxide nanoparticle was added directly to the in vitro culture and injected into mice.

2.2.6. Cellular cytotoxicity

For assessing intracellular toxicity of iron oxide nanoparticle, a colorimetric assay, 3-(4,5-dimethylthiazol-2-yl)-2,5-diphenyltetrazolium bromide (MTT), was performed. HepG2 cells (2 × 10 [4]) were seeded in a 96-well plate separately. Cells were treated with iron oxide nanoparticle at different concentration (25, 50, 100 μg/mL) and grown in an incubator (37°C and 5% CO2) for 24 h. Cells were washed and 10 μL of MTT with a concentration of 5 mg/mL was added in each well. After 3 h of incubation, 100 μL of dimethyl sulfoxide (Sigma-Aldrich) was added to each well. The absorbance was measured by a Multi-Mode Plate Reader (Bio-Rad) at 595 nm. The percentage of survival was calculated as follows -

$$\% \text{ cell survival} = 100 \times \frac{\text{average OD of treated cells}}{\text{average OD of control cells}}$$

To determine the cytotoxicity of iron oxide nanoparticle (ATA-IONP) and the combination of iron oxide nanoparticle with artesunate (ATA-IONP+ART), the release of enzyme lactate dehydrogenase (LDH) from damaged cells was measured. Briefly, Raw 264.7 cells (2×10 [4]) were seeded in clear bottom 96-well plate. Cells were treated at different concentrations with ATA-IONPs (0–200 μg/mL) and combination ATA-IONP+ART (100 μg/mL ATA-IONP + 0.2–10 nM ART). After 48 h incubation, the plate was gently shaken to ensure homogenous distribution of LDH in the culture medium. Cells were centrifuged at 600 ×g for 10 min and supernatant (10 μL/well) was transferred to a new plate having 100 μL LDH reaction mix. Lyophilized LDH dissolved in LDH reaction mix served as a positive control. The solutions were mixed well and absorbance was read at 450 nm by Multi-Mode Plate Reader (Bio-Rad). Percent cytotoxicity was calculated as follows –

$$\% \text{ cytotoxicity} = 100 \text{ x } \frac{\text{Test sample} - \text{Low control}}{\text{High control} - \text{Low control}}$$

2.2.7. Growth inhibition assay

To determine more efficient inhibition on parasite growth, compounds were tested at different concentrations against *P. falciparum* strain 3D7. Briefly, Initial synchronization was carried by purifying schizonts on a percoll gradient followed by tight synchronization using sorbitol.

The culture at the late ring to early trophozoite stage (18–22 h) of 0.8% parasitemia and 2% hematocrit was incubated with varying concentrations of iron oxide nanoparticle (0–200 μg/mL) alone and artesunate (0.0125–10 nM) with or without 100 μg/mL iron oxide nanoparticle for one cycle (48 h). Untreated culture served as control. Following incubation, thin smears for each sample were methanol fixed & stained with Giemsa. Over three thousand RBCs were scored for each slide to determine the parasitemia. Experiments were performed as three biological replicates, each $N = 3$.

To evaluate the advantage of using iron oxide nanoparticles over iron supplements as a source of ferrous ion, growth inhibition assay was carried. The culture at the late ring to early trophozoite stage (18–22 h) of 0.8% parasitemia and 2% hematocrit was incubated with varying concentrations of artesunate (0.025–10 nM) with 100 μg/mL iron oxide nanoparticle and with Fe_2SO_4 (source of ferrous ion) for one cycle (48 h). Untreated culture served as control. Following incubation, thin smears for each sample were methanol fixed & stained with Giemsa. Over two thousand RBCs were scored for each slide to determine the parasitemia. Experiments were performed as three biological replicates, each $N = 3$.

Growth inhibition (% Inhibition) was calculated as follows:

$$\% \text{ inhibition} = 100 \text{ x } \frac{(\%\text{parasitemia of control} - \%\text{parasitemia of treated})}{\%\text{parasitemia of control}}$$

2.2.8. Hemolysis assay

Defibrinated human blood (3 mL) was collected and centrifuged at 1500 rpm for 10 min. RBC pellet was purified by successive washing (thrice) with PBS (0.01 M phosphate buffer and 0.9% NaCl) and diluted 6 times. Diluted RBCs (300 μL each) were treated with varying concentration of iron oxide nanoparticles alone (25, 50, 100, 150 and 200 μg/mL) and the combination with artesunate (100 μg/mL ATA-IONP +0.2–4 nM ART) for 3 h at 37 °C. After centrifugation, the supernatant was collected and the absorbance of the hemoglobin released was read at 540 nm using UV − visible spectrophotometer (Bio-Rad 680, USA). All the experiments were performed in triplicates. Percent hemolysis was calculated with respect to hemolysis caused by negative control

(PBS) and positive control (De-ionized water), as shown in the following equation:

$$\% \text{ hemolysis} = 100 \text{ x } \frac{\text{sample 540nm} - \text{negative control 540nm}}{\text{positive control 540nm} - \text{negative control 540nm}}$$

2.2.9. Progression assay

Tightly synchronized, ring stage culture (6–8 h) was diluted to 1.5% parasitemia & 2% hematocrit to determine any delay in progression upon treatment. Briefly, each well with 1.5% parasitemia and 2% hematocrit was treated with or without artesunate (2 nM) in the presence or absence of 100 μg/mL iron oxide nanoparticle for 48 h. Untreated cells served as control. To evaluate any morphological and progression variation, Giemsa stained smears were prepared at respective time points 22, 44, 52 and 60 h. Nearly 2000 cells were scored by light microscopy. The relative percentage frequency of different stages of parasite ring, trophozoite, and schizont (R, T, S) was inferred by the pie diagram.

2.2.10. Ring survival assay

Efficacy of surface coated iron oxide nanoparticles+artesunate on artemisinin-resistant parasites was determined by Ring survival assay (RSA). The *in vitro* assay was performed as described by Witkowski et al. [32] and Worldwide Antimalarial Resistance Network (WWARN) (2013) [33]. The assay was performed using two transgenic *P. falciparum* 3D7 parasite isolates bearing either wild type artemisinin-sensitive marker PfKelch13[WT] (WT) or artemisinin-resistant mutation PfKelch13[R539T] (R539T). These parasite lines were generated as described in Mbengue et al.[34] Briefly, parasite cultures were percoll purified and tightly synchronized, 0–3 h post invasion rings at 1% parasitemia with 2% hematocrit were incubated with artesunate alone (2 nM IC50x1 and 700 nM IC50x350) and artesunate in combination with iron oxide nanoparticles (100 μg/mL) for 6 h. The cultures were washed thoroughly with 10 mL of cRPMI twice to remove the drug, resuspended in fresh complete medium and incubated for the next 66 h. Thin blood smears for each treated and untreated culture were Giemsa stained at 6 h and after 72 h. >10,000 RBCs were scored for each experiment. Experiments were performed thrice in triplicates. Mean parasitemia and growth rate was determined and the survival rate was calculated as follows:

$$\% \text{ of survival rate} = 100 \text{ x } \frac{\text{Artesunate exposed parasitemia at 72 h}}{\text{non} - \text{exposed parasitemia at 72 h}}$$

2.2.11. Cellular uptake assay

Intracellular uptake was studied using NHS-FITC-tagged iron oxide nanoparticle. To incorporate FITC tag, iron oxide nanoparticle was mixed with NHS-fluorescein (NHS-FITC) and bath sonicated for 2 min. The reaction was set overnight at 37 °C. Unlabelled FITC was removed by centrifugation. The synchronized culture at different stages ring, trophozoite, and schizont maintained with 4% parasitemia and 2% hematocrit in 24 well plates was incubated with FITC tagged iron oxide nanoparticle for 6 h. Smear for each stage was drawn and methanol fixed followed by nuclear staining with DAPI. Cells were examined under Nikon Ti2 eclipse fluorescent microscope at 100× magnification.

Localization of iron oxide nanoparticles within the acidic vacuole of the parasite was observed by live cell imaging using lysotracker Red. Live asynchronous Pf3D7 culture with 5–6% parasitemia and 2% hematocrit was supplemented with overnight FITC tag incorporated iron oxide nanoparticles. The culture was incubated with tagged iron oxide nanoparticles for 6 h at 37 °C. LysoTracker Red DND-99, a pH-based dye for staining the food vacuole and Hoescht 33,342, a DNA based dye for nucleic acid staining was added to the culture at the concentration of 100 nM for 1 h and 10 μg/mL respectively. Cells were washed with 0.01 M PBS and drop cast on a glass slide with a coverslip and

examined under Nikon A1R confocal microscope using 60× magnification. Serial z-sections with step sizes of 0.4 μm were gathered using sequential scanning. The laser transmitted light differential interference contrast (DIC) images were collected at an optimum z-level separately. Image stacks, co-localization was analyzed using NIS-element software and deconvoluted z-stacks were reconstructed in 3D using IMARIS software, version 6.4.2 or 7.0.0 (Bitplane Scientific) to enable proper visualization and interpretation.

2.2.12. Intracellular reactive oxygen species (ROS) detection by DCFDA

With the known effect of artesunate to generate ROS, an increase in the ROS generation in the presence of iron oxide nanoparticle was studied. Synchronized and purified parasites of late trophozoite stage with 3% parasitemia and 2% hematocrit was incubated with 20 μM DCFDA for 30 min. Later parasites were treated with artesunate (2 nM) in the presence or absence of iron oxide nanoparticle (100 μg/mL) for 3 h. Untreated infected RBCs with or without iron oxide nanoparticle (100 μg/mL) was used as a control. The fluorescence intensity was measured by imaging in Nikon Ti2 eclipse fluorescence microscope at 100× magnification. Mean fluorescence intensity was calculated for 20 cells each and compared relatively.

2.2.13. DNA damage by comet assay

The single-cell DNA damage was studied for *P. falciparum* using comet assay [35]. Briefly, sorbitol synchronized parasites (~4 × 10⁶) in their trophozoite stage (24–28 h) were treated with ATA-IONPs (100 μg/mL), ART (4 nM) and ART+ATA-IONPs accordingly. Parasites were collected by centrifugation after 6–8 h, lysed with 0.01% saponin and washed with ice-cold phosphate-buffered saline (1xPBS). Cells resuspended in 1xPBS were diluted with 300 μl 0.8% low-melting-point agarose (LMPA) and cast on precoated slides (1% normal melting point agarose - NMPA). Cells were coated with another layer of 0.8% LMPA and incubated with chilled lysis solution for 1 h at 4 °C. Followed by alkaline lysis treatment for 30 min, electrophoresis was performed at 1 V/cm with current 300 mA, in an alkaline solution for 30 min. Slides were neutralized upon incubation in neutralization solution for 10 min followed by fixation in chilled 70% ethanol (5–10 min), rinsed in distilled water and dried overnight. Slides were rehydrated and stained with ethidium bromide (10 μg/mL). Images of comets were captured in Nikon eclipse Ti2 fluorescent microscope at 40× magnification. Comets were scored using Image J – Open Comet software. To determine the extent of DNA damage, olive tail moment (OTM) was calculated for each sample and compared.

2.2.14. Protein carbonylation by DNPH assay

To determine oxidative species-mediated protein damage, the extent of protein carbonylation was studied using DNPH assay [36,37]. Basically, synchronized parasites (8–10%) of late rings to early trophozoite stage (18–22 h) were treated with ATA-IONPs (100 μg/mL), ART (4 nM) and ART+ATA-IONPs accordingly. RBCs were collected by centrifugation after 6–8 h, lysed with 0.01% saponin. Parasite pellets were washed with 1xPBS, lysed with RIPA buffer and treated with 1% streptomycin sulfate to remove nucleic acids. All the samples were prepared in duplicates. Uninfected RBCs with similar treatments served as host control. Proteins in the supernatant from each sample were derivatized for an hour with 500 μL of 10 mM DNPH in 2 M HCl. Sample controls were also prepared by adding an equal volume (500 μL) of 2 M HCl. Proteins were precipitated with 20% TCA. Pellets were centrifuged and washed with ethanol: ethyl acetate mixture (1:1) to remove unbound DNPH. The pellet was dissolved in 500 μL of 6 M guanidine hydrochloride. Carbonyl content was determined by reading the absorbance at λ = 370 nm for each sample against an appropriate blank. The absorbance of bovine serum albumin (BSA) dissolved in 6 M guanidine hydrochloride at 280 nm was used to plot a standard curve and calculate the total corrected protein in the final step of the reaction.

The protein carbonyl concentration (nmol/mL) was calculated by -

$$\text{Protein Carbonyl}\left(\frac{\text{nmol}}{\text{mL}}\right) = \left[\left(\frac{\text{A370nm}}{0.011}\right) * \left(\frac{500\,\mu\text{L}}{500\,\mu\text{L}}\right)\right]$$

Average carbonyl content (nmol/mg) was calculated by –

$$\text{Carbonyl content}\left(\frac{\text{nmol}}{\text{mg}}\right) = \frac{\text{Protein carbonyl}\left(\frac{\text{nmol}}{\text{mL}}\right)}{\text{Corrected protein concentration}\left(\frac{\text{mg}}{\text{mL}}\right)}$$

2.2.15. In vivo growth inhibition assay

In vivo growth inhibition was studied by injecting mice with *P. berghei* ANKA as mentioned above [38]. Briefly, PbA infected female Swiss albino mice (8–10 weeks old) were divided into following seven groups ($N = 3$): ART (6 mg/Kg), ATA-IONPs + ART (6 mg/Kg), ART (30 mg/Kg), ATA-IONPs + ART (30 mg/Kg), ART (60 mg/Kg) as positive control, only ATA-IONPs and infected mice without any treatment as negative control. The dosage of ATA-IONPs was kept constant as 5 mg/Kg body weight. The first dose of the drug with nanoparticle was injected intraperitoneally (IP) to the desired groups when the parasitemia was observed in the blood of infected mice (Day 3). When the parasites observed were early rings around 6 h post invasion (hpi) the drug was administered followed by five days consecutively. Parasitemia was determined every day by scoring ~3000 RBCs from tail blood smear of each mice. Experiments were performed twice ($N = 3$ for each group) and growth inhibition was determined as discussed before.

2.2.16. In vivo histopathology studies

In vivo cytotoxicity of the combination (ATA-IONPs+ART) was assessed by histopathological studies. Uninfected healthy female mice were injected with 30 mg/Kg ART and 5 mg/Kg ATA-IONPs for 5 consecutive days. Similar experimental conditions were maintained as above. The general behavior, touch response and other aspects of mice was monitored for 21 days followed by sacrifice and dissection. Liver, kidney, spleen, and brain were isolated. Organs were fixed in 10% formalin and slides were stained with hematoxylin and eosin (H&E). Slides were observed for cellular changes; tissue damage or depositions and their morphology was analyzed.

2.2.17. Statistical analysis

Student's *t*-test for unequal variances was performed to evaluate significant differences between treatment and control samples. *P*-value <.05 and *p*-value <.01 were considered significant (*P*-values are mentioned on the graph respectively). Results represent the mean ± SD of a minimum of three independent experiments, each performed in triplicates.

3. Result

3.1. Synthesis and characterization of surface coated iron oxide nanoparticle

The IONPs were synthesized by aqueous co-precipitation of iron salts in alkaline medium, (Fig. 1a). The so formed NPs were stabilized with 2-aminoterephthalic acid (ATA) at a mild temperature to form organic coated IONPs (ATA-IONPs). The formation of ATA-IONPs was confirmed by UV–visible spectroscopy, XRD and thermogravimetry analysis. A control iron oxide nanoparticle without ATA coating was also synthesized to assist the analysis.

3.1.1. Nature of NPs

The phase of nanoparticles was confirmed by powder-XRD analysis, (Fig. 1b). Uncoated IONPs showed a high-intensity peak at 2theta = 32.56 ° corresponding to (420) plane [JCPDS no. #00–016-0653] along with the other characteristic XRD peaks confirming the co-existence of magnetite and maghemite (Fe_2O_3) structures suggesting oxidation of Fe^{2+} ions to Fe^{3+} ions under the synthetic conditions. ATA-IONPs revealed the crystal planes (110), (220), (311), (512), (400) confirming the inverse spinel structure of Fe_3O_4 phase. The peaks of synthesized ATA-IONPs matched with the magnetite (Fe_3O_4) NPs, PDF data [JCPDS no. 01–086-1343]. The non-existence of peak at (420) in ATA-IONPs confirmed the existence of Fe^{2+} ions and their stability against aerial oxidation due to the presence of the coating [39]. Such stability in oxidation states of iron ions is essentially required to ease the processing and administration of drug formulations.

3.1.2. The existence of coating

The uncoated Fe_3O_4 nanoparticles showed a broad featureless UV–vis. Spectrum, Fig. 1c. On the contrary, ATA-IONPs clearly displayed two characteristic peaks at 220 nm and 330 nm which is accounted to the π-π* and n-π* transition associated with ATA functionalities confirming the existence of coating on nanoparticles.

3.1.3. Amount of coating

The percentage coating in ATA-IONPs was determined by Thermogravimetry analysis (TGA). IONPs are invariable thermally stable as compared to ATA-IONPs, Fig. 1d. Two mass loss is clearly observed in ATA-IONPs, in the temperature range 100–200 °C and 200–800 °C. The initial mass loss is accounted to the evaporation of water, whereas the latter mass loss is due to the decomposition of the organic surface coatings (ATA) on the IONPs [40]. The amount of surface coating on ATA-IONPs was determined as ~22% based on the basis of comparative residual mass obtained in both the IONPs at 800 °C.

3.1.4. Size and morphology

SEM (Fig. 1e) and TEM (Fig. 1h) images of ATA-IONPs illustrated NPs have a spherical shape. Similar to other magnetic NPs, ATA-IONPs exhibited agglomerated state due to their magnetic nature accounting heterogeneity in size [30]. SEM images revealed the difficulty in determination of particle size of synthesized NPs. However, TEM analysis of NPs clearly showed an average particle size of 10 nm with a homogeneous size distribution of the nanoparticles. The selected area electron diffraction (SAED) pattern confirms high crystallinity of the sample with diffraction rings associated due to their stacking to each other due to their magnetite phase. The energy-dispersive X-ray spectroscopy (EDS), studies again reconfirm the existence of organic coating due to structurally rich nitrogen and carbon percentages along with the substantial percentage of iron, (Fig. 1f-g).

3.1.4.1. pH- responsiveness of ATA-IONPs.

Chemically, Fe^{2+} release from ATA coated iron oxide nanoparticles was quantified through o-phenanthroline assay at different pH (5.0, 6.0 and 7.4, using PBS buffer)
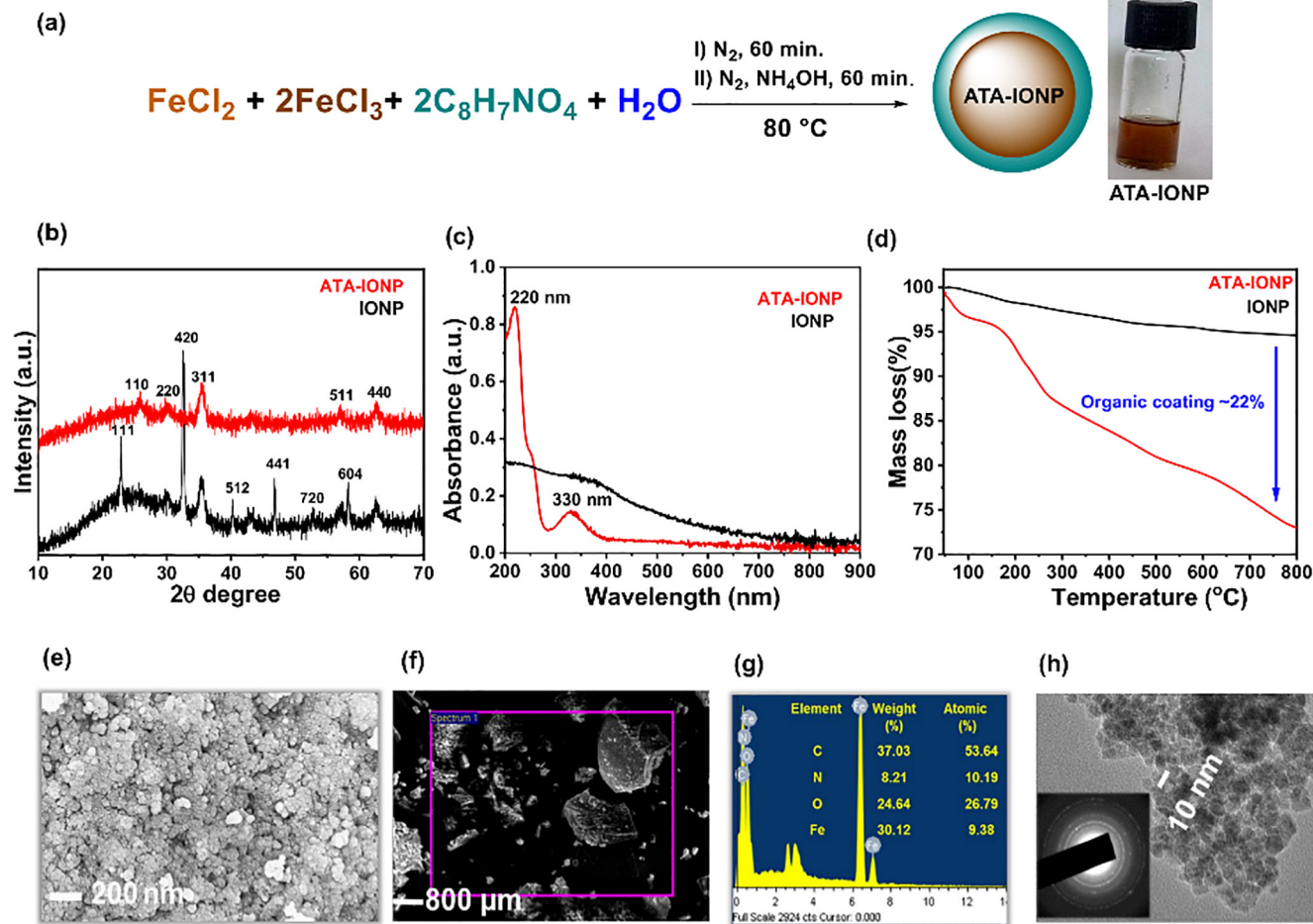

Fig. 1. Characterization of ATA-IONPs. (a) Synthetic scheme of 2 − amino−terephthalic acid coated iron oxide nanoparticles (ATA-IONPs), with digital images of their aqueous suspension (2.5 mg/mL), (b) Powder-XRD spectra, (c) UV–visible spectra, (d) Thermogravimetric analysis of coated ATA-IONPs and uncoated IONPs (control sample), (e) Representative FESEM of ATA-IONPs, (f-g) EDS mapping of respective region of ATA-IONPs and % atomic composition confirming the presence of organic ATA coating on IONPs in the selected area zone and (h) TEM image showing the spherical shape morphology and inset shows selected area electron diffraction (SAED) pattern exhibiting the crystalline domains.

values with variation in time, Fig. 2a. The pH was chosen to represent the physiological environments inside the cell. A pH-dependent release of iron ions as Fe^{2+} is observed, which is higher at lower pH. This suggests the pH-mediated release of iron ions from the nanoparticles. At pH value of 7.4, no noticeable effect on the release of Fe^{2+} ions is observed with time confirming their stability. Additionally, a sustained release of iron ions is observed at lower pH (< 7.4) values. A slow release occurred within an initial 12 h followed by a plateau. To ascertain this behavior of NPs, TEM images were recorded at the same pH values. It can be visualized in Fig. 2b, ATA-IONPs existed as aggregates and clusters at neutral (pH 7.4) with an average size of 18.31 ± 2.08. In contrast, in weakly acidic PBS (pH 6.0) ATA-IONPs existed as less closely bound structures with an average size of 10.86 ± 1.277, Fig. 2b. However, upon further increasing the acidic conditions (pH 5.0), an enhancement in loosely bound nanoarchitecture along with the release of smaller particle size nanoparticles is observed (average size of 5.05 ± 0.54), Fig. 2b. However, the hydrodynamic size of nanoparticles (Fig. 2c) showed a reverse trend from 215 ± 23 nm (pH 7.4) to 380 ± 33 nm (pH 5). This accounts for the change in surface energy of nanoparticles due to their surface coating. The existence of ATA-IONPs in free-state is supportive for the detection of more release of Fe^{2+} species as observed in phenanthroline assay. A sustained release of free Fe^{2+} is desired for enabling the enhanced and prolonged activity of the drug. The efficacy of artesunate is essentially regulated by the Fe^{2+} ion concentration to enable the Fenton type reaction to cleave the peroxide linkage and mediate enhancement in ROS levels [41].

3.1.4.2. Intracellular uptake of iron oxide nanoparticles in infected RBCs.
Cellular internalization of iron oxide nanoparticle was explored in *Plasmodium*-infected RBCs by labeling ATA-IONPs with NHS-fluorescein (NHS-FITC). After incubating with ATA-IONPs-FITC for 6 h, cells were methanol fixed and counterstained with DAPI and observed under Nikon Ti2 eclipse fluorescence microscope. As shown in Fig. 3a, parasite nuclei are stained blue by DAPI. Besides, bright green fluorescent spots are clearly observed in the cytoplasm of infected cells. This verifies readily uptake of the nanoparticle by infected RBCs. The overlay of fluorescence images also depicts green fluorescence closely around the food vacuole confirming the intracellular Nano-carrier ability of the ATA-IONPs. Further localization of the iron oxide nanoparticles within the food vacuole was confirmed by the live cell imaging along with the acidic compartment-specific dye Lysotracker red. Fig. 3b clearly depicts colocalization of NHS-FITC tagged ATA-IONPs within the acidic organelle in the parasites. For a better visualization purpose, similar images were also reconstructed by 3-D imaging. Fig. 3c and mov. 1 illustrates 3-D images along with the *Z*-section of Lysotracker Red and FITC-tagged ATA-IONPs getting specifically colocalized within the food vacuole with close proximity to the hemozoin.

3.1.4.3. Enhanced efficiency of artesunate activity by iron oxide nanoparticles against parasite growth. With known efficacy of artesunate as an intraerythrocytic antimalarial drug, we used nanoparticle-based enhancement for its activity. To evaluate the efficiency of iron oxide nanoparticles, synchronized late stage rings were treated with increasing concentration of artesunate along with 100 µg/mL ATA-IONPs. GIA was performed for one cycle (48 h) with parasitemia assessed by scoring the Giemsa stained slides. To negate the effect of iron oxide nanoparticle alone on parasite growth, a similar assay was performed with the late ring stage parasites for one cycle with varying concentration (0–200 µg/mL) of ATA-IONPs.

The effect of nanoparticle was nearly constant in the range 80–200 µg/mL of ATA-IONP (Fig. 4c). Thus, with negligible cytotoxicity (Fig. 4b) and higher cellular compatibility (Fig. 4a), we proceeded further studies with 100 µg/mL ATA-IONPs. Also, in these experiments, nanoparticle alone did not affect the parasite growth post one cycle
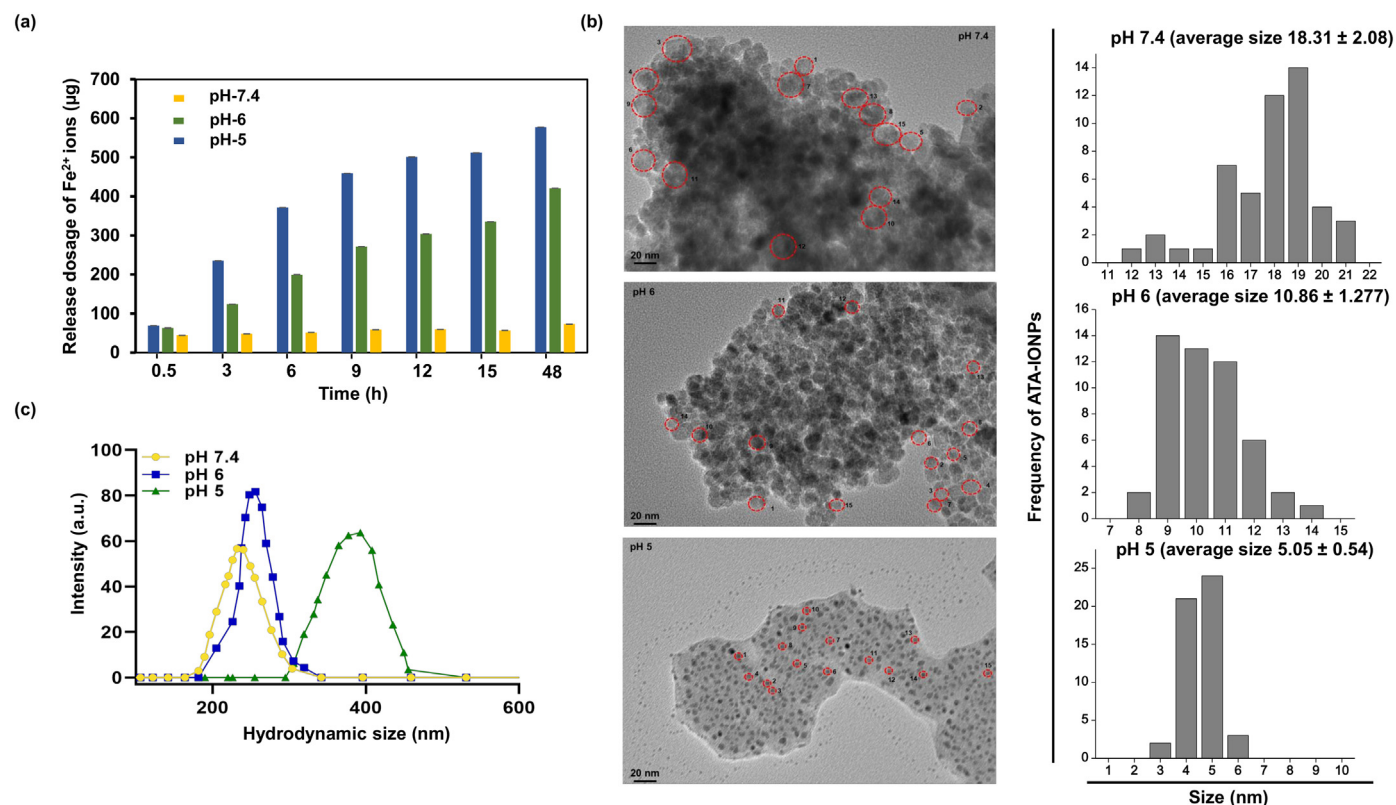

Fig. 2. The pH-responsive release of Fe^{2+} from the surface coated ATA-IONPs. (a) Quantitative analysis of the Fe^{2+} released from ATA-IONPs at different pH environments, (data represents the mean ± standard error of the mean of three independent experiments) and (b) the corresponding representative TEM images of ATA-IONPs in 1xPBS buffer at different pH values 7.4, 6.0, and 5.0. The diameter of the ATA-IONPs was estimated from 50 particles each which are free from the aggregated state. Data represent the mean ± standard error of the diameter of 50 particles each. (c) Hydrodynamic size of NPs at respective pH.
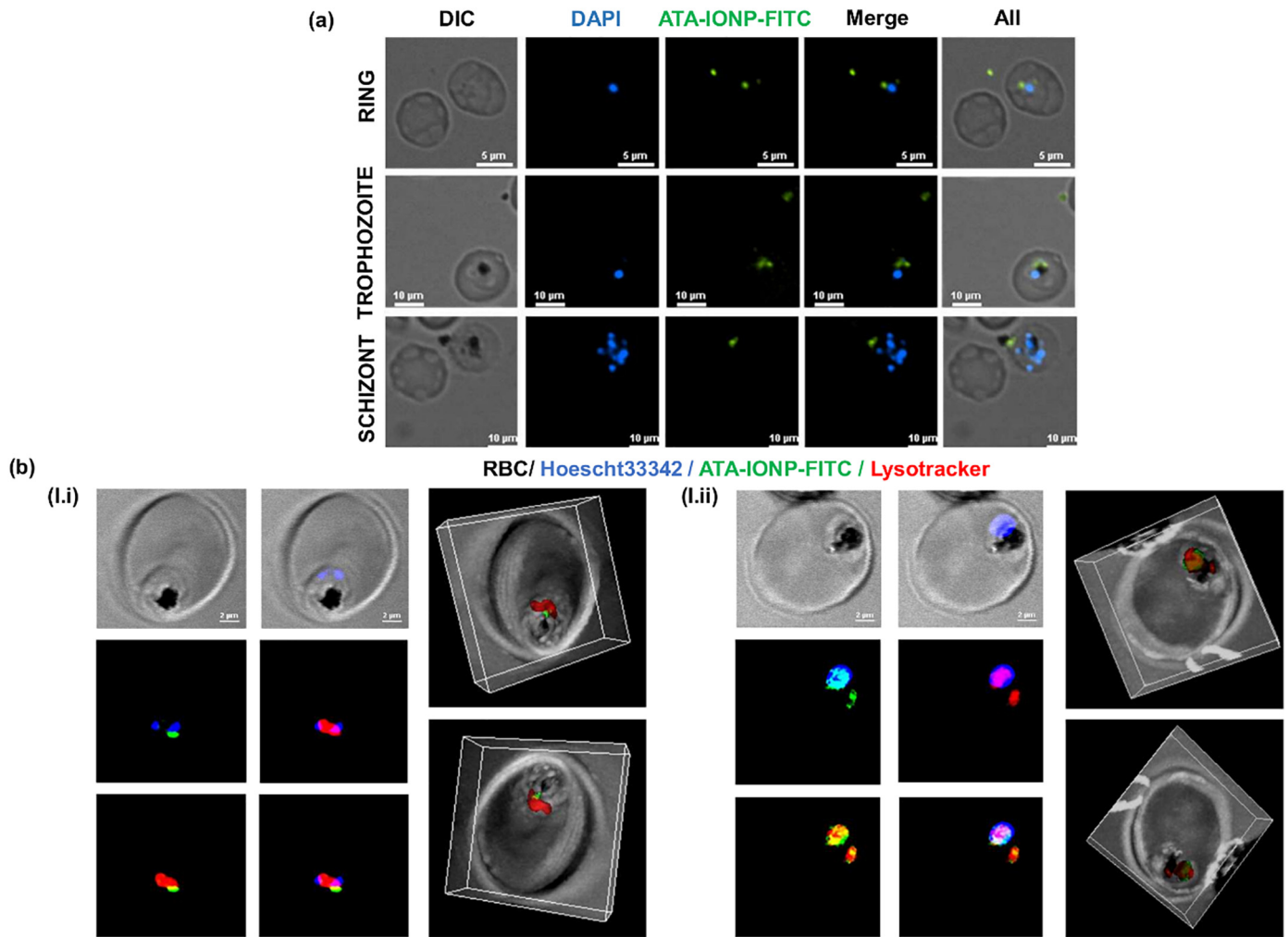
Fig. 3. Specific accumulation and uptake of surface coated ATA-IONPs in *P. falciparum*-infected RBCs. (a) ATA-IONPs were co-incubated with NHS-FITC overnight at 37 °C for labeling and unlabelled FITC was removed. FITC labeled ATA-IONPs were incubated with infected parasites for 6 h, smears were prepared by methanol fixation and examined by fluorescent microscopy (magnification 100×). Cellular uptake of FITC labeled ATA-IONPs (green) is visible in all three intra-erythrocytic stages of parasite near the food vacuole. The nucleus of the parasites is labeled with DAPI (blue). (b) To analyze the localization of ATA-IONP-FITC in the food vacuole, the parasites were stained with lysotracker red (100 nM) for 1 h. Colocalization of ATA-IONP (green) within the acidic compartment labeled with Lysotracker (red) was visualized by confocal microscopy (magnification 60×). The nucleus of the parasites is labeled with hoescht 33,342 (blue). The deconvoluted z-stack images of ATA-IONP and lysotracker were further reconstructed in 3-dimension with IMARIS software for better visualization. (see supplementary movie 1 and 2 for z stacks)

(Fig. 4c). However, the results (Fig. 4d) demonstrate that iron oxide nanoparticle together with artesunate depicted reduced parasite load in a dose-dependent manner. Treatment of *P. falciparum* with artesunate exhibited IC$_{50}$ value of 2 nM as reported previously [42]. Upon screening the combinatorial treatment of artesunate with iron oxide nanoparticle, a nearly 5-fold decrease in the *in vitro* inhibitory concentration of artesunate was observed. The growth inhibition level is higher (~0.4 nM) for ATA-IONPs+ART as compared to artesunate alone (~2 nM).

A further advantage of the combination of artesunate with surface coated iron oxide nanoparticle over simple iron (ferrous) supplements was assessed by performing comparative GIA for one cycle. Previous studies have related the use of Fe$_2$SO$_4$ *via* iron supplements as a readily available source of free ferrous ions [20,22]. In this experiment Fe$_2$SO$_4$ (800 μM) was used as the source of a ferrous ion at a concentration similar to ferrous ions in 100 μg/mL ATA-IONPs. Our results corroborate with previous studies [20,22] with a marginal increase in the parasitemia when treated with Fe$_2$SO$_4$ while the negligible effect was observed upon treatment with ATA-IONPs, suggesting the non-toxicity of surface coated ATA-IONP despite being an iron source. Upon screening, the combination of Fe$_2$SO$_4$ + ART decreased the *in vitro* inhibitory concentration of artesunate by 3-fold (~0.6 nM) (Fig. 4e). However,

the combination of ATA-IONP+ART decreased the *in vitro* inhibitory concentration of artesunate by 5-fold (~0.4 nM), relatively proving it to be significantly more efficacious than Fe$_2$SO$_4$ + ART (Fig. 4e). Since Fe$_2$SO$_4$ is a ready source of freely available iron, it may lead to non-specific artesunate activity attributing sudden outburst of artesunate. Thus, with minimal growth inhibition of iron oxide nanoparticles, the result supports a better inhibitory effect of ATA-IONPs+ART on malarial parasite growth.

Cytotoxicity of ATA-IONPs against human cells was determined at a different concentration of ATA-IONPs (25, 50 and 100 μg/mL) upon incubation with Human liver hepatocellular carcinoma cells (HepG2). Post 24 h incubation no cellular death was observed (supplementary fig. 1b). Additionally, cytotoxicity of ATA-IONPs and their combination ATA-IONP+ART was also studied in macrophagic Raw 264.7 cells. Post 48 h incubation marginal cellular damage was observed in both ATA-IONP alone and combination treated cells (Fig. 4b). Like their cytocompatibility, the nanoparticles were analyzed for the hemocompatibility against human erythrocytes. Concentrations ranging from 25 to 200 μg/mL ATA-IONPs and the combination of 100 μg/mL ATA-IONP with varying concentration of ART yielded <10% hemolysis, signifying them hemocompatible (Fig. 4a).
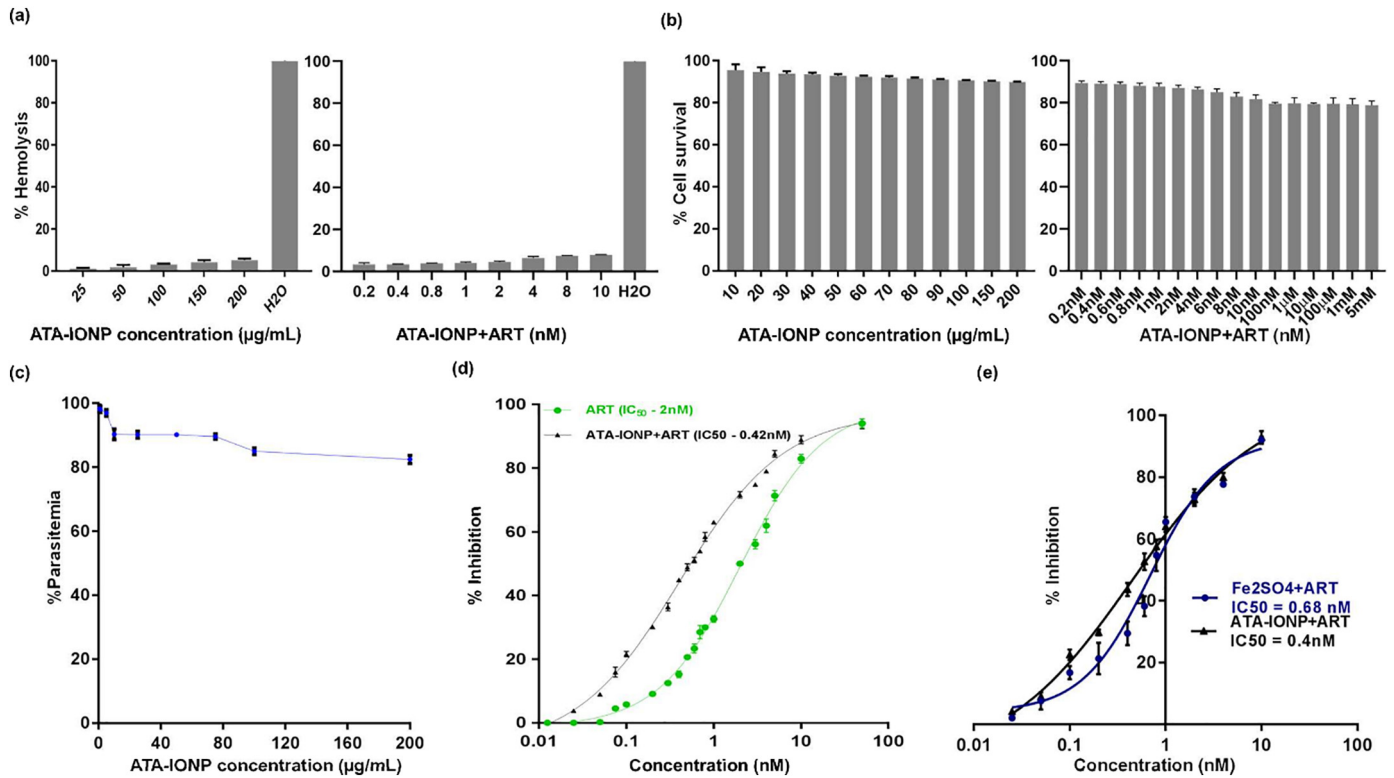
Fig. 4. Cellular compatibility of ATA-IONP and ATA-IONP+ART with human RBCs and Raw 264.7 cells and its effect on *P. falciparum* growth. (a) Compatibility of the combination of ATA-IONP with ART and ATA-IONPs alone with healthy human RBCs was determined by treating freshly isolated RBCs with varying concentration of ATA-IONPs (0–200 μg/mL) and 100 μg/mL ATA-IONP + (0.2–4 nM) ART for 3 h. Hemoglobin release was measured to evaluate the hemocompatibility of these nanoparticles where H_2O and 1xPBS served as a positive and negative control. (b) Raw 264.7 macrophagic cells were treated with the combination of ATA-IONP with ART and ATA-IONPs alone for 48 h at different concentrations (0–200 μg/mL) and (100 μg/mL ATA-IONP +0.2–10 nM ART) respectively. Percent cytotoxicity was measured with LDH assay where untreated cells served as control. (c) Surface coated ATA-IONP of varying concentrations (0–200 μg/mL) were incubated with *P. falciparum* infected RBCs for 48 h. Infected RBCs without nanoparticles served as control. Giemsa stained smears were scored for parasitemia and the percent parasitemia showing the negligible effect of nanoparticles alone on parasite growth is represented in the graph. (d) Infected RBCs were treated with varying concentrations of artesunate (0.0125–10 nM) with or without 100 μg/mL ATA-IONP for one intra-erythrocytic cycle (48 h). Untreated parasite culture served as control. The parasitemia was scored on Giemsa stained smears and iron nanoparticle-mediated enhanced inhibition activity of artesunate on *P. falciparum* growth was determined. (e) Infected RBCs were further treated with varying concentrations of artesunate (0.025–10 nM) with 100 μg/mL ATA-IONP and with Fe_2SO_4 (source of ferrous ion) for one intra-erythrocytic cycle (48 h). Untreated parasite culture served as control. The parasitemia was scored on Giemsa stained smears and enhancement in the inhibition activity of artesunate for both the combinations was determined. The effect of artesunate fortification was found to be significant with P value 0.008. Data represents as means ± SD of three independent experiments (n = 3). Statistical analyses were done with student's *t*-test for unequal variances. P-value (student's *t*-test for unequal variances) <0.05 and < 0.01 were considered significant.Data represents as means ± SD of three independent experiments (n = 3).

3.1.4.4. Significant repression of parasite growth by ATA-IONP+ART combination.

After deducing the inhibitory concentration for the combination, a stage-specific effect on *in vitro Plasmodium* growth was studied. Morphological and growth defects were analyzed by counting ~3000 cells/Giemsa stained smears in duplicate. Parasites from early rings were monitored every 6 h post infection (hpi) until one cycle (48 h). Post one cycle, infected RBCs with and without nanoparticle treatment, both of which served as a control, had healthy mid rings (Fig. 6a). As evident, treatment with 100 μg/mL iron oxide nanoparticles yielded healthy mid rings likely to the morphology of untreated parasites.

In comparison, parasites treated for the same duration with artesunate as well as combination rendered delay in the growth cycle. The growth of the parasite delayed from ~ 44 h in artesunate-treated cells while they remained stalled at ~ 52 h in combination treated. As shown in (Fig. 6a) both the artesunate & combination treated cells exhibited a population of parasites with pyknotic morphology. Degenerative populations of trophozoite, as well as schizont stage in combination, treated parasites rendered further delay in the intraerythrocytic growth. As a result, 60 h combination treated parasites unveiled punctate schizonts in comparison to mid rings in control cells.

With vital differences observed at ~ 60 h, untreated parasites and nanoparticle treated parasites had relatively 80–90% late rings. However, as shown (Fig. 6a) artesunate treated had (59%) late rings with crisis morphology while the combination treated population had (~6%)

rings. Clearly indicating the improved lag upon combination treatment in the stage-specific growth of *Plasmodium*.

Furthermore, (Fig. 6b) clearly supports the significant growth inhibition upon combination treatment with radically reduced parasitemia as compared to artesunate treated cells. Hence, results again validated the efficiency of the iron oxide nanoparticle to improve the efficacy of the drug artesunate.

3.1.4.5. Enhanced efficiency of artesunate towards artemisinin resistant parasites by ATA-IONP+ART combination.

Utilization of artemisinin and its derivatives (artesunate) in ACTs rather than as a monotherapy is chiefly attributed to its short half-life and sudden outburst of its activity, rendering the development of slow clearing parasites (drug-resistant ones) [43]. The artemisinin-resistant strains have been shown to be resistant for this therapy because of its slow clearance rate. This slow clearance phenotype of the dormant resistant parasites is hard to analyze *in vitro*. However various experimental set up has been suggested to study this resistant phenotype. Ring survival assay (RSA) as described by Witkowski et al. [32] analyzes the drug-resistant phenotypes of the *Plasmodium*. In the RSA parasites are treated for a shorter time and after thorough washing, the survival rate is analyzed post 72 h. To examine the effect of ATA-IONP+ART combination on the *P. falciparum* resistant line, RSA was performed on the slow clearing parasites (resistant type R539T) and its susceptible counterpart fast clearing parasites (wild type). The combination of ATA-IONP+ART yielded enhanced efficacy of

artesunate on resistant and sensitive strains similar to its effect on Pf3d7. Fig. 5 illustrates the result of RSA for wild type and artemisinin-resistant strain R539T at two different concentration of artesunate (2 nM and 700 nM) in the presence or absence of ATA-IONPs. The result shows a significant difference upon combination treatment in the survival rate of both fast as well as slow clearing parasites at 6 and 72 h. The combination of ATA-IONP+ART enhanced the efficacy of artesunate by 3.3-fold and 5.4-fold in resistant strain R539T at 2 nm and 700 nM. While the efficacy of artesunate was enhanced by 4.9-fold and 8.1-fold in *P. falciparum* WT strain. Very interestingly, level of clearance rate in R539T was improved upon 6 h and 72 h treatment of ATA-IONP+ART. These results thus suggest the ability of ATA-IONP to radically enhance the activity of artesunate and provide improved clearance of both artemisinin sensitive and artemisinin-resistant strains.

3.1.4.6. Elevation of endoperoxide mediated oxidative stress level in infected RBCs by ATA-IONP+ART combination. Based on literature studies, intracellular ROS generated mode of parasite death is known for artemisinin and its derivatives (artesunate) [42]. Previous studies already suggest the formation of potentially toxic free radical intermediates when artemisinin reacts with the free oxidized form of iron (Fe^{2+}) within infected RBCs [44]. With this ideology, we studied the effect of the iron oxide nanoparticle to enhance the liberation of free radicals *via* artesunate. Intracellular ROS level was measured *via* H_2DCFDA assay in the purified late stage trophozoites. Parasites treated with and without ATA-IONPs served as control. As shown (Fig. 7) untreated malarial parasite had minimal ROS while 100 μg/mL iron oxide nanoparticles treated parasites exhibited nearly marginal ROS levels. Artesunate (2 nM) induced ROS in *P. falciparum*-infected RBCs effectively while an enhanced increase of ~1.5fold in the ROS level was observed in combination treated *Plasmodium*-infected RBCs.

An increase in the ROS level in terms of mean fluorescence intensity (MFI) of DCFDA was observed in artesunate + iron oxide nanoparticle treated parasites as compared to artesunate alone (Fig. 7). The increase in the MFI was measured from 331.48 MFI in artesunate alone to 506.39 MFI in artesunate + iron oxide nanoparticles respectively (*p*-value 0.017). These results suggest the combination of iron oxide nanoparticles + artesunate enhanced the activity of artesunate by elevating the oxidative stress level in infected RBCs.

3.1.4.7. Extensive intracellular DNA damage in malaria parasites by ATA-IONP+ART combination. Increased free radical formation by artesunate is well known in *Plasmodium* species [42]. Previous studies have evaluated intracellular DNA damage related to the death of parasites by artesunate using comet assay. Artesunate-treated cells showed a comparative increase in the measure of the olive tail moment (OTM) [(42)]. To evaluate whether the combination (ATA-IONPs+ART) results in a surplus ROS based DNA damage compared to ART alone, sorbitol synchronized trophozoites were treated with ART (4 nM), with or without ATA-IONPs (100 μg/mL). The DNA damage was visualized by comet assay and quantified by measuring the OTM of individual cells. As seen in Fig. 8a control cells had no comet while parasites treated with ATA-IONPs exhibited little comet tailing. However, ATA-IONPs+ART treated cells had a significant increase in tail DNA as compared to ART-treated cells alone. To assess the extent of DNA damage, we scored comets for their migration pattern (average olive tail moment). Fig. 8a illustrates that ATA-IONPs+ART treated parasites demonstrated higher DNA damage shown by an increase in the olive tail moment (OTM). Treatment of parasites with ATA-IONPs alone for 6–8 h didn't unveil any detectable DNA damage. While ART treatment (4 nM) for 6–8 h resulted in increased DNA damage like previous studies [(42)]. However, exposure of parasites to the combination for the same duration (6–8 h) increased

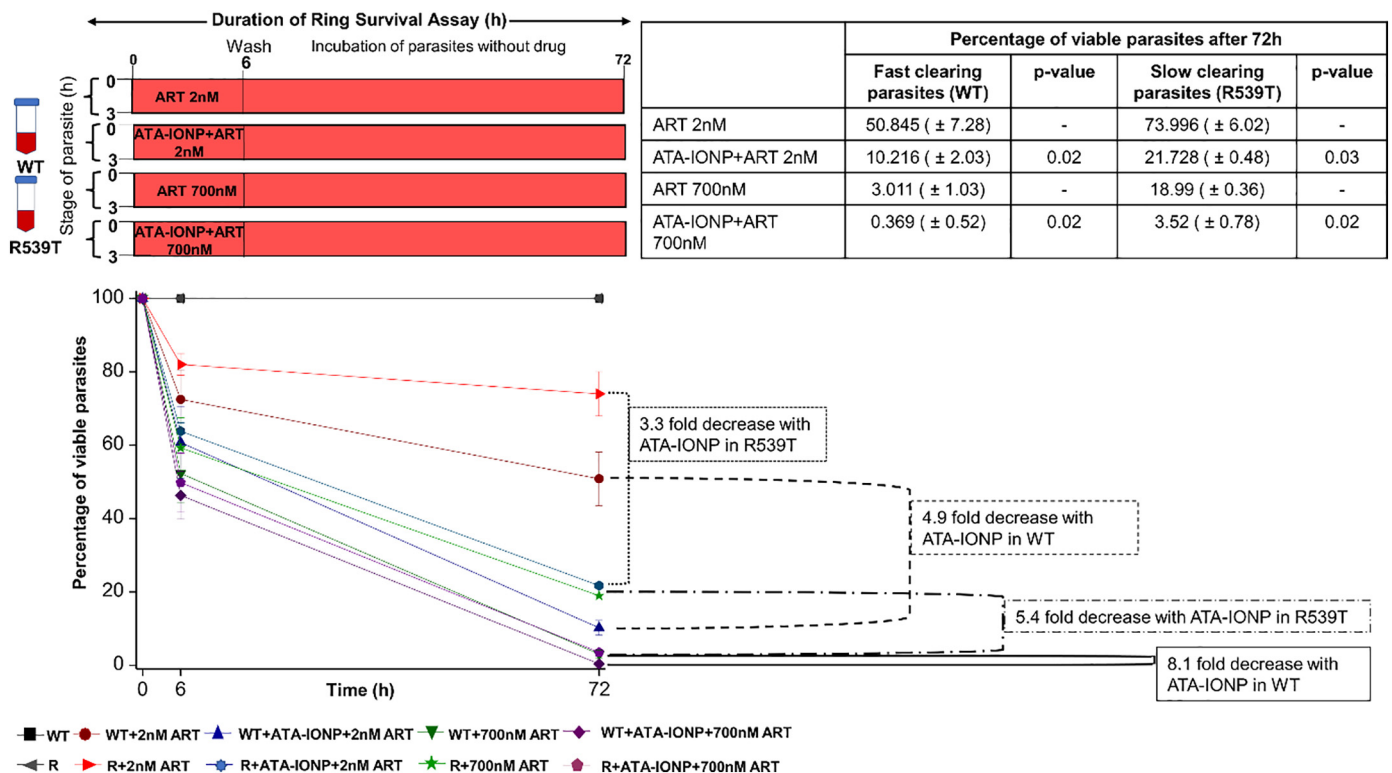|		Percentage of viable parasites after 72h			
		Fast clearing parasites (WT)	p-value	Slow clearing parasites (R539T)	p-value
	ART 2nM	50.845 (± 7.28)	-	73.996 (± 6.02)	-
	ATA-IONP+ART 2nM	10.216 (± 2.03)	0.02	21.728 (± 0.48)	0.03
	ART 700nM	3.011 (± 1.03)	-	18.99 (± 0.36)	-
	ATA-IONP+ART 700nM	0.369 (± 0.52)	0.02	3.52 (± 0.78)	0.02

Fig. 5. Sensitization of artesunate resistant parasites with ATA-IONP+ART combination. Efficacy of surface coated ATA-IONP+ART on artemisinin-resistant parasites was determined by Ring survival assay (RSA). *In vitro*, a tightly synchronized culture of 0–3 h rings was treated with artesunate alone (2 nM IC50x1 and 700 nM IC50x350) and artesunate in combination with ATA-IONP (100 μg/mL) for 6 h. After thorough washing with 10 mL cRPMI twice, the parasites were further cultured in fresh medium without drug pressure for the next 66 h. Enhanced activity of artesunate towards artemisinin-resistant *P. falciparum* strain (R539T) and the wild type Pf3D7 strain (WT) was determined by scoring >10,000 RBCs per experiment. Experiments were performed thrice in triplicates. The combination of ATA-IONP+ART in R539T resulted in 3.3-fold and 5.4-fold decrease in percent survival at 2 nM and 700 nM ART respectively. Data represented as means ±SD (n = 3). Statistical analyses were done with student's t-test for unequal variances. P-value (student's t-test for unequal variances) <0.05 and < 0.01 were considered significant.

the extent of DNA damage (OTM) specifically in the parasitized cells enormously. These results suggest, the sustained release of Fe^{2+} from ATA-IONPs indeed results in greater efficacy of the drug ART.

3.1.4.8. Carbonylation facilitated irreversible protein damage in ATA-IONP +ART treated parasites. Alteration in the protein backbone or modifications in the amino acid side chains is well-studied damages contributed by increased intracellular ROS. Many diseases utilize these oxidized proteins as biomarkers for oxidative stress. One of the modifications includes the carbonylation of the protein side chain [(45)]. To determine the extent of protein carbonylation, the protein fraction of cellular lysates from treated trophozoite stage parasites were derivatized with DNPH. Fig. 8b shows parasites treated with ATA-IONPs alone exhibited carbonylation like control. While parasites treated with ATA-IONPs+ART exhibited excessive protein carbonyl content as compared to ART alone. However, in contrary nanoparticles along with the drug displayed negligible protein carbonylation in the host cells (Fig. 8b), indicating the elevated ROS mediated protein damage to be specific to the parasites. The result further validates the ability of ATA-IONPs to enhance the activity of ART against parasites. Since nanoparticles display slow release of Fe^{2+}, ATA-IONPs alone manifested subtle changes in parasite ROS level contributing minute intracellular damages. However, the specificity of the surface coated nanoparticle to target majorly infected erythrocytes remains unknown.

3.1.4.9. Enhanced efficacy of artesunate in P. berghei infected mice by ATA-IONP+ART combination. To investigate the increased *in vivo* efficacy of ATA-IONPs+ART, growth inhibition was studied in PbANKA infected mice. As shown in Fig. 9a parasite load steadily increased in untreated and ATA-IONPs alone treated mice. However, Fig. 9a also shows a reduced load of parasites in infected mice supplied with ART alone while combination treated mice had significantly reduced parasite load. We could clearly observe that in combination 30 mg/Kg ART and 5 mg/Kg ATA-IONPs showed the same antimalarial activity as 60 mg/Kg dose of ART alone. Conversely, groups receiving ART at 30 mg/Kg dose alone showed 60% inhibition till day 7 while at 6 mg/Kg dose alone we observed around 30% inhibition. Furthermore, on day 7 combination of ART with ATA-IONPs reduced the dosage of ART ~10 times inhibiting the parasite growth by 80%. Results thus indicated, a combination of ATA-IONPs with ART promisingly elevated the activity of the potent antimalarial drug. In addition, histological studies performed for the combination (30 mg/Kg ART and 5 mg/Kg ATA-IONPs) on several organs such as brain, kidney, lung, and spleen from injected and un-injected healthy mice depicted very mild infiltration of mononuclear cells. (Fig. 8b and supplemental Fig. 2).

4. Discussion

The Chinese herb artemisinin is proven to be therapeutically potential against malaria and several other infectious diseases such as hepatitis B [46], schistosomiasis [47], and numerous types of cancers [48,49]. The semi-synthetic artemisinin (artesunate) which is more soluble, is a remarkable antimalarial drug, however, its lower efficacy in blood has been a major concern. *In vivo,* the drug gets metabolized immediately upon administration, resulting in an outburst of its activity with high plasma level [50]. Rapid activation can be attributed to the iron-mediated opening of a lactone ring, resulting in complete exposure of endoperoxyl functional group. This can be overcome by slow release of the catalyst Fe^{2+} within the cells thereby activating artesunate (ART) in a sustainable manner. Upon administration, the pro-drug artesunate gets activated in the presence of Fe^{2+} within the cells. This sudden activation of the drug is catalyzed by iron-mediated cleavage of the endoperoxide bridge resulting in the formation of toxic free radicals. Such non-specific activation can be avoided by providing a controlled and targeted release of the catalyst (Fe^{2+}) for the drug. Here in, we have considered the approach where surface coated IONPs at

acidic pH slowly converts ferric to ferrous ions providing a sustainable release, leading to persistent activation of artesunate, enabling the generation of radical species *via* endoperoxide cleavage.

Lower efficacy of the drug has been a major setback leading to recrudescence and parasite resistance. Upon injection, due to low plasma stability, artesunate gets activated in the plasma prior to reaching the target site which might result in low efficacy. To prolong the timeframe of release, encapsulation of ART in nanocapsules, liposome, complexing with cyclodextrins, *etc.* have already been used [50–52]. These studies did improve ART activity by decreasing the diffusion and enabling controlled release. Secondly, the efficacy of ART can also be improved in the presence of Fe^{2+}. As per the literature, selective toxicity of ART towards cancer cells has been attributed to high iron content within cancer cells [53]. Similarly, in *Plasmodium*, the impact of iron level for ART has been supported by Meshnick et al. [3] where they showed a similar iron dependency of ART in *Plasmodium*-infected RBCs. These studies further indicate the dependency of ART activity on iron. Herein, we have tried to improve the efficacy of ART by providing the Fe^{2+} catalyst in a very slow and sustainable manner from ATA-IONPs. Both *in vivo* and *in vitro*, artesunate along with the nanocarrier exhibited dose-dependent antimalarial activity. ATA-IONPs+ART showed much higher inhibition of parasite growth than the drug alone while nanocarrier had a negligible effect on the parasite growth. Next, the cytocompatibility of ATA-IONPs +ART with a range of concentrations used in our study was tested for hemolysis and cytotoxicity assay in Raw 264.7 cells. ATA-IONPs+ART at a concentration of 0.2–10 nM yielded <10% hemolysis and < 20% cytotoxicity. The effect of cytotoxicity did not change further and remained constant even at the range of 10 μM to 5 mM artesunate with 100 μg/mL ATA-IONP, proving the better cytocompatibility of the combination even at these higher concentrations as well. In contrary, to compare the efficacy of iron oxide nanoparticles with artesunate, a combination of iron supplement (Fe_2SO_4) with artesunate was used. Despite ~3fold reduction in the inhibitory dosage of artesunate, a combination of Fe_2SO_4 + ART proved to be less efficacious as compared to ATA-IONP+ART. Also, being a readily available source of free $Fe2+$, utilization of Fe_2SO_4 can render non-specific drug activation rather than a regulated drug activity. Herein, utilizing the concept of $Fe2+$ release but in a sustained pH-dependent manner our formulation of surface coated iron oxide nanoparticles with artesunate proved beneficial. These findings support the unavailability of free ferrous ions (Fe^{2+}) for rapid parasite growth from the surface coated iron oxide nanoparticles (Fig. 4c-e). Our current study also signifies the strategic approach of utilizing surface coated iron oxide nanoparticles to enhance the activity of artesunate towards resistant strains. Studies have clearly indicated the development of recrudescence for artemisinin and derivatives in regions of South East Asia. This phenomenon of recrudescence attributed to delayed parasites clearance has been associated with *in vitro* study of ring stage survival assay [32]. The dormancy of the parasites at the ring stage is associated with reduced hemoglobin digestion and tolerating ART pressure [54]. Our study of ring survival assay suggests the efficient enhancement in the activity of artesunate in the presence of slowly releasing catalyst ($Fe2+$) towards both sensitive and resistant strains of *Plasmodium* (Fig. 5).

Both ART and parasite require iron in the ferrous state. However, in erythrocytes, elemental iron in the labile iron pool chiefly acts as the source of iron. Use of iron nanoparticles as a source of Fe^{2+} seems to be effective, however, IONPs such as (Fe_2O_3, Fe_3O_4) act as a direct source of Fe^{2+} rendering iron overexposure to the drug and the parasite. Thus, the sudden outburst of the drug though eliminates parasite burden fails complete clearance, enabling the parasite to utilize ferrous ions for cellular activities and multiply. Therefore, the slow release of the ferrous iron from the surface coated iron oxide nanoparticle in combination treated parasites showed higher efficacy of artesunate to stall the parasite growth (Fig. 6).

Previous studies have also shown the use of surface coated iron oxide nanoparticles such as Ferumoxytol which have promisingly low

toxicity, low degradation, the null effect on cellular function and viability [55]. In our study, we have utilized FDA approved 2-aminoterephthalic acid coated superparamagnetic iron oxide nanoparticles as a source of Fe^{2+} to enhance ART efficacy (Fig. 1). The physicochemical characterizations, especially the size of NPs, revealed a pH-dependent reduction in the size of ATA-IONPs (TEM images, Fig. 2b, 18.31 ± 2.08 to 5.05 ± 0.54). On the contrary, hydrodynamic size of nanoparticles showed a reverse trend (Fig. 2c, 215 ± 23 nm to 380 ± 33 nm) which can be accounted to the change in surface energy of nanoparticles due to highly polar nature of the surface coating. Cellular uptake of NPs depends on nature, shape, size, surface charge, and nature of coating on NPs. It is also dependent on the dose, and type of cell used [56]. It is reported that particles with diameter dimensions of 50–80 nm have direct access to intraerythrocytic parasites. While size $> \sim 100$–150 nm has shown a relatively lesser extent than smaller sizes [57]. In general, there is a size-dependent uptake of NPs via endocytosis in surface coated nanoparticles. The mechanism of intake of NPs can be via membrane-wrapping process or passive transport, which allows entry of particulates of various sizes. In our case, there is variation in the size of NPs with the pH as indicated by in vitro experiments. However, due to the multicomponent nature of in vivo conditions, we expect, besides size dependency, other parameters may guide cellular uptake. Once entered, understanding its mode of activity, demands further studies in this direction.

The NPs with iron ions in its core and an organic layer on its surface do not activate ART upon interaction. Presence of iron ions in the core of ATA-IONPs prevents its reduction, inhibiting drug activation. Fig. 2a and Fig. 2b denotes the pH-dependent kinetic release of Fe^{2+} from our ATA-IONPs. Maximum release at pH 5.0 acts as an added advantage in the case of malarial activity. Free liberation of individual NPs at acidic pH, mostly at pH 5.0 enables sustained release of Fe^{2+}. Quantification of Fe^{2+} ions released from the nanocarrier, exhibited ~10fold increase in the release at pH 5.0 while pH 6.0 exhibited ~6-fold increase with respect to pH 7.0 (~1 fold). Additionally, the slow kinetic release of Fe^{2+} in the parasite boosts the controlled release and activity of the drug. During the trophozoite stage, the digestive vacuole of the parasite acts as the depot for all metabolic activities and few of the antimalarials concentration within this compartment is already known. Since the acidified vacuole has a physiological pH -5.0, it is being the destination for most of the drug [58]. Interestingly, we also observed microscopically the internalization of our ATA-IONPs within the parasite cytoplasm with proximity to the food vacuole during ring and trophozoite stage. The ATA-IONPs specifically co-localized within the lysotracker stained acidic food vacuole of Plasmodium. This observation supports the targeted delivery of the nanocarrier within the food vacuole of infected RBCs (Fig. 3 and supplementary mov. 1,2). Also, targeted delivery and selectivity of ATA-IONPs for infected RBCs over uninfected RBCs remains elusive.

In Plasmodium iron-dependent artesunate exerts its activity through ROS by damaging cellular macromolecules. Damage to these biomolecules such as protein and DNA via free radicals is its chief mechanism of action. In the previous study, Gopalakrishnan et al. [42] had already provided substantial evidence for ROS mediated DNA damage by ART in Plasmodium falciparum. In the present study, we observed the combination of ATA-IONPs+ART elicited the enhanced generation of ROS in the presence of iron catalyst than ART alone (Fig. 7). Mechanistically,
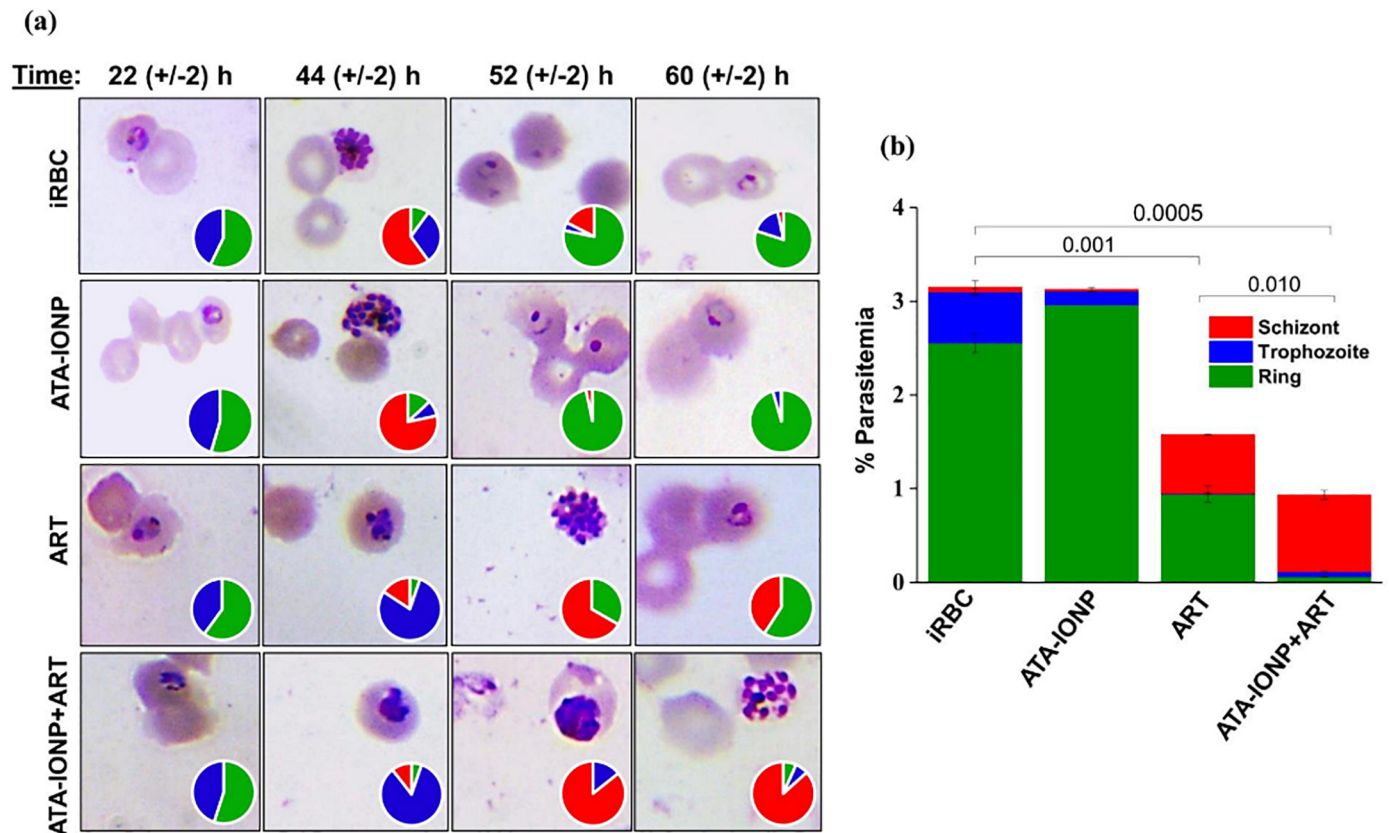

Fig. 6. In vitro efficacy of ATA-IONPs to boost the activity of ART against P. falciparum. Effect of ATA-IONPs to boost ART activity w.r.t Plasmodium growth was determined by progression assay. Infected parasites at their ring stage were treated with 100 μg/mL ATA-IONPs with artesunate (2 nM), artesunate alone (2 nM) and 100 μg/mL ATA-IONPs alone for 48 h. Giemsa stained smears were prepared at various time points 22, 44, 52 and 60 h. Panel (a) shows light microscopy images at different time points for varying treatments. Pie charts depict relative proportions of rings, trophozoites, and schizonts stages of P. falciparum. (b) Correlation between progression delay and repressed parasite growth studied post one cycle. The following interpretation is used - ring (green) trophozoite (blue) and schizont (red). Nearly 6000 RBCs scored, and the data is representative of two independent experiments. Statistical analyses were done with student's t-test for unequal variances. P-value (student's t-test for unequal variances) <0.05 and < 0.01 were considered significant.

we also observed under these conditions when the ROS level was high, the extent of DNA damage was also significantly high. Parasites treated with the combination (ATA-IONPs+ART) exhibited significantly much higher tail length than artesunate alone (Fig. 8a). This profound DNA damage caused by nanoparticle drug combination demonstrated the enhanced antiparasitic activity. Another macromolecular damage that gets targeted due to enhanced ROS level is protein damage.

Concomitant protein damage and DNA damage is a result of cellular vandalism by oxidative radicals. Carbon and oxygen-centered radicals released after bioactivation of artesunate inflict parasite protein alkylation and adduct formation. A major hallmark of protein damage is alkylation of proteins regulated by varying enzymes within the host and the parasite. However, in *Plasmodium*, metabolically active trophozoite and late ring stages cultivate a highly oxidative environment. Several antimalarials such as Chloroquine, artesunate are known to be involved in metal-catalyzed oxidation, causing carbonylation based protein damage. Proteomic profiles of these drugs (Chloroquine) post carbonylation elucidated several proteins belonging to the protein folding, protein fate, energy metabolism, signal transduction, and pathogenesis [59]. Recently, Wang et al. [60] unraveled the random targets of artemisinin upon heme driven activation. This study enlightened the core mechanism of action of artemisinin with their dependency on iron degradation. A study by Ismail et al. [61] contributed the potential plasmodial proteins that get alkylated following adduct formation. The study scrutinized oxidative damage specific targets of the drug and determined the endoperoxome. With protein carbonylation being an irreversible modification, damages incurred are lethal. Despite these recent studies, it remains unclear if artemisinin and its derivatives carry carbonylation as their measure of oxidative damage within *Plasmodium falciparum* and

the specific proteins that get carbonylated needs to be identified. With the pervasiveness of this drug, we evaluated the enhanced protein damage specific to carbonylation in the parasite. In this study, the extent of carbonylation was investigated by DNPH assay wherein, the carbonylated proteins get derivatized with 2,4-dinitrophenylhydrazine (DNPH). The degree of protein carbonylation is proportional to the concentration of carbonyl content measured. Using DNPH as a label, our results (Fig. 8b) indicate the parasite treated with the combination elicited enhanced carbonyl content in comparison to artesunate alone. We also analyzed the effect of artesunate and nanoparticle-based modifications in the host RBCs and found no change. These results (Fig. 8b) strongly suggests that protein damage through carbonylation is much more prevalent in ATA-IONPs treated parasites than artesunate alone and are not contributed from the host. As expected, like other observations, the substantial release of the drug and catalyst from the nanoparticles caused extensive carbonylation of parasite proteins in contrast to host proteins. Further insightfulness may be gained by carrying the proteomic profile of those proteins that get carbonylated.

To further evaluate the efficiency of the nanoparticle as a potential agent to deliver and boost the drug efficacy, we investigated the *in vivo* effect in mouse malaria model of *Plasmodium*. A comparative efficacy study showed the ability of nanoparticles to augment artesunate activity in *P. berghei* infected mice (Fig. 9a). In combination treated mice parasitemia was affected at significantly low drug dosage (~8–10 fold) as compared to artesunate alone. The present work illustrates a dose of artesunate as low as 6 mg/kg combined with 5 mg/kg ATA-IONPs, showed a profound ability to inhibit PbA parasitemia by ~85% by day 7. The similar increase in artesunate efficacy both *in vivo* and *in vitro* showed the significance of this study. Since previous studies have
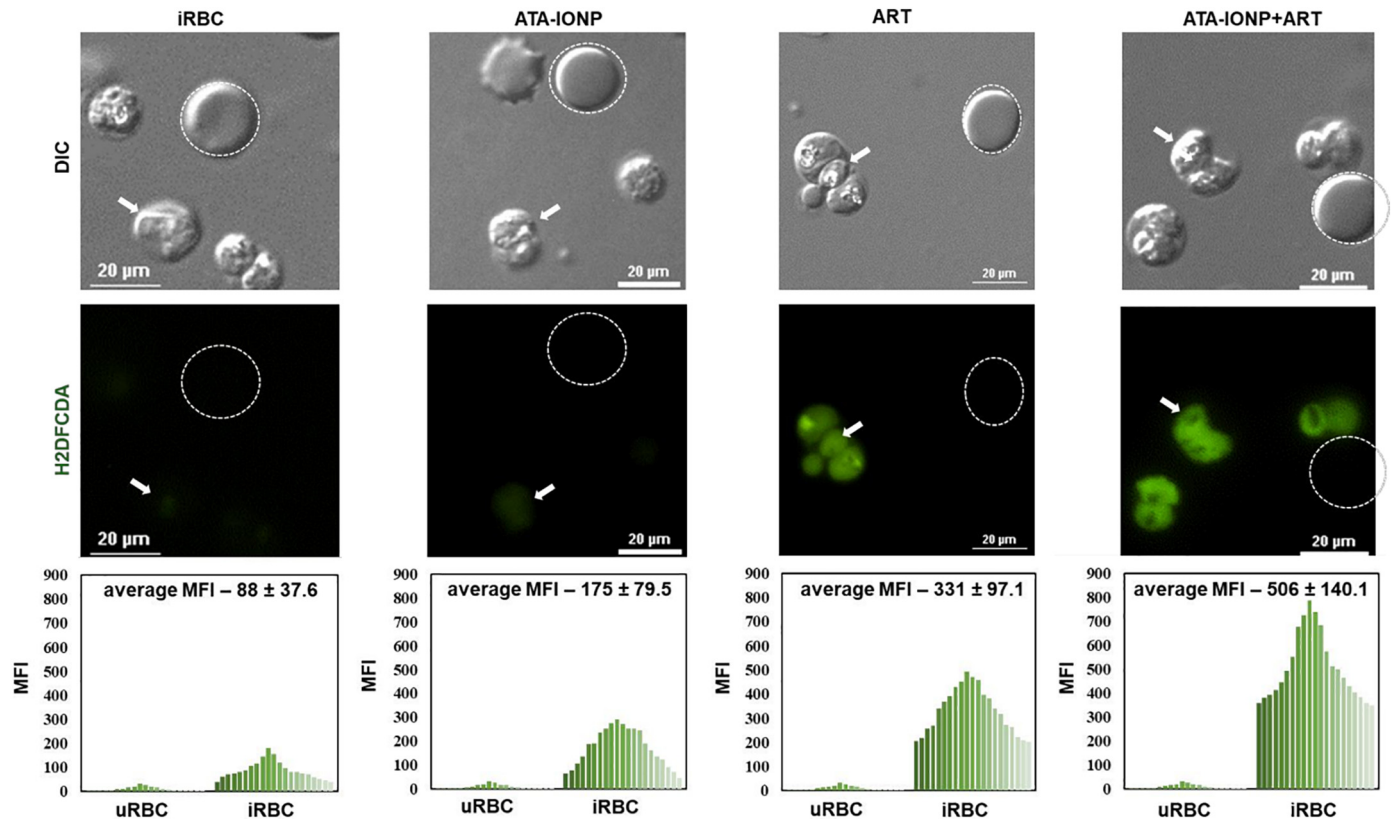

Fig. 7. Iron oxide nanoparticle combination maximizes oxidative stress level in *P. falciparum* parasite. Increase in intracellular reactive oxygen species (ROS) level was monitored by H2DCFDA assay. *Plasmodium*-infected RBCs with 3% parasitemia were treated with or without 100μg/mL ATA-IONPs in the presence and absence of ART (2 nM) for 3 h. Prior to nanoparticle and drug treatment, infected RBCs were pretreated with 20 μM DCFDA for 30 min. Images were captured in Nikon Ti2 eclipse fluorescent microscopy (magnification 100×). The graphical representation shows mean fluorescent intensity (MFI) for DCFDA fluorescence between uninfected and infected RBCs for each set of treatment. An enhanced fluorescence signal in ART-treated cells in the presence of iron oxide nanoparticle is observed in comparison with that of ART alone. The difference between the MFI of ART and ATA-IONP+ART is statistically analyzed by students t-test and was found to be significant (*p*-value 0.017).
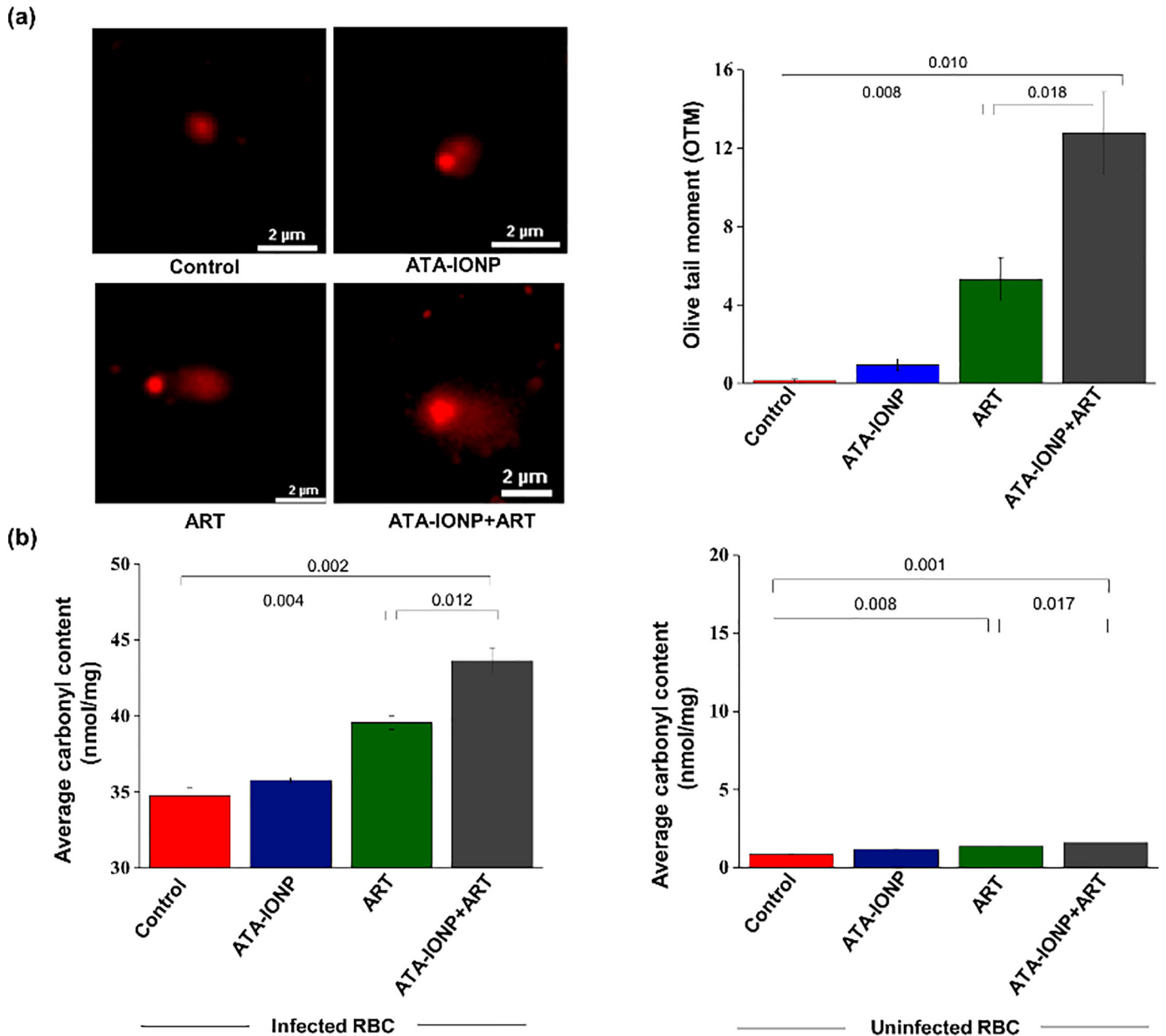

(a)

(b)

Fig. 8. Artesunate and ATA-IONPs combination markedly magnifies the cellular damages in *P. falciparum* infected RBCs. To visualize the DNA and protein-mediated damages, RBCs were infected with (~4 × 10⁶) parasites in trophozoite stage and treated with or without ATA-IONPs (100μg/mL) in the presence or absence of ART (4 nM) for 6–8 h. Post-treatment DNA from treated parasites were run in a sandwich of low and high melting point agarose gel. The DNA damage was assessed by comet assay. Panel (a) shows DNA damage in the form of extended tail length for the comet formed. Untreated parasites served as control. The graph depicts the quantitative measurement of an olive tail moment (OTM) to estimate the extent of DNA damage in all samples. (n = 25) Image of comets was scored for each sample. The error bars represent ±SD. Protein damage was determined by DNPH assay. Protein carbonyl content (nmol/mg of total protein) within the infected parasite proteins and the host proteins were compared. Panel (b) indicates an increase in protein carbonylation in combination treated parasites as compared to untreated parasites (infected RBCs). The graph shows the negligible effect on protein carbonylation within the host proteins. All the experiments were done in triplicates with error bars representing ±SD. Statistical analyses were done with student's t-test for unequal variances. P-value (student's t-test for unequal variances) <0.05 and < 0.01 were considered significant.

reported the iron oxide nanoparticles to be toxic, hematoxylin and eosin stained tissue samples of a healthy mouse injected with 30 mg/Kg artesunate and 5 mg/Kg ATA-IONPs were examined. Brain, kidney, lung, and spleen of injected and control mice were analyzed for cellular changes, tissue damage or depositions, and their external morphology. Very slight infiltration of mononuclear cells was observed in treated mice (Fig. 9b and supplemental fig. 2). These infiltrations may represent some slightly triggered antigenic response upon administration of the combination. Moreover, no chronic immune characteristics, signs of distress such as behavioral changes were observed.

In conclusion, this study for the first time paved the way in employing a particle-mediated approach to enhance the efficacy of

ART. Surface coated nanoarchitecture of ATA-IONPs resulted in effective and sustained drug delivery along with its catalyst (Fe²⁺), enhancing the therapeutic potency of artesunate. This encapsulation conceals IONPs and artesunate, thereby circumventing their non-specific interactions. The presence of ATA-IONPs in free-state within the food vacuole (pH ~5.0) regulates ART activity, facilitating Fenton type reaction, targeting irreversible modifications in *Plasmodium* biomolecules. The results demonstrate significantly high efficacy of the artesunate with an evidently reduced dosage in *P. falciparum* fast clearing (WT) and slow clearing (R539T) parasite strains. This study can leave a unique possibility open for utilizing ATA-IONPs to reduce parasite relapse, also to prolong the efficacy of ART against ART-resistant malaria
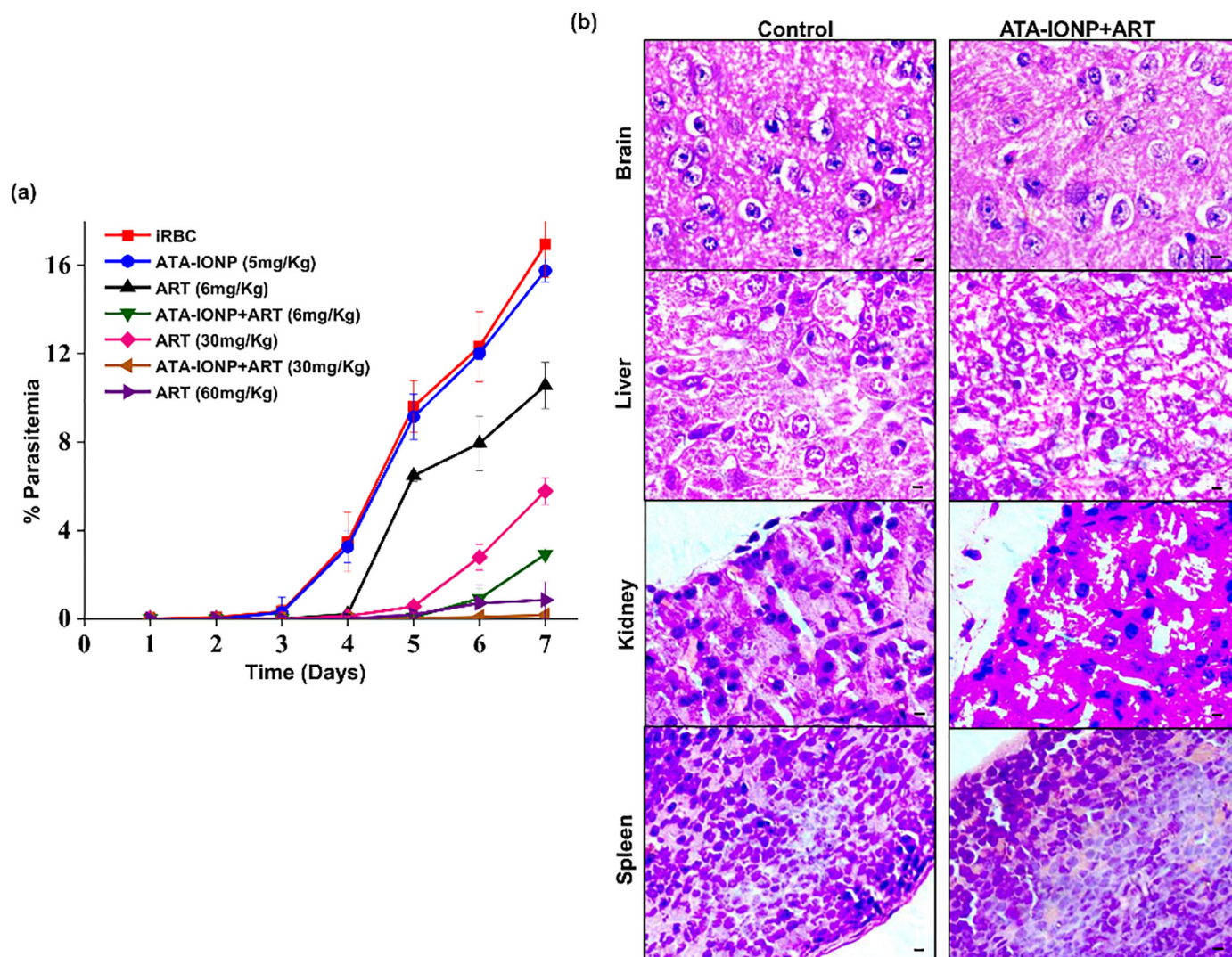
Fig. 9. *In vivo* combination therapy mediated rapid decrease in parasitemia and its toxicity. (a) *In vivo* effect of ATA-IONPs, ART, ATA-IONPs+ART was studied in *P. berghei* infected mice. Nanoparticles and the drug combination [+] or [−] were injected intraperitoneally in mice for 5 consecutive days. Infected mice without any treatment served as control. A dosage of 5 mg/Kg body weight of ATA-IONPs and 6 mg/Kg, 30 mg/Kg, 60 mg/Kg of ART was used. Parasitemia was monitored every day by drawing smear from tail blood of each mice. The graph represents the growth rate of *Plasmodium* upon treatment for 7 consecutive days. Experiments were performed in duplicates with (n = 3 for each group). (b) *In vivo* toxicity of combination ART (30 mg/Kg) + ATA-IONPs (5 mg/Kg) visualized by Hematoxylin and eosin (H&E) staining of tissue samples obtained from injected healthy mice. Tissue samples from uninfected healthy mice served as control. No tissue damages were observed after administration of nanoparticle. Magnification of 100× has been illustrated in the figure. Scale bar: 10 μm. The error bars represent ± SD.

parasites. This study presents a promising and robust therapeutic outlook for improvising artesunate activity to safeguard the human population against dreadful malaria.

Declaration of interests

D. Kannan reports she was supported by Shiv Nadar Foundation fellowship for the work and has nothing to disclose. N. Yadav reports she was supported by Shiv Nadar Foundation fellowship for the work. S. Ahmad reports he was supported by Indian Council of Medical Research (ICMR) fellowship for the work. P. Namdev has nothing to disclose. Dr. Bhattacharjee has nothing to disclose. Dr. Lochab reports experimental funding from Shiv Nadar University. Dr. Singh reports grants from NIH and DST-INDIA during the conduct of the study.

Author contributions

Study concept and design: SS, DK; acquisition of data: DK, NY, SA; Analysis and interpretation: SS, DK, BL, NY; drafting of the manuscript: SS, DK, Bl, and NY. BL and NY have taken care of nanomaterial section; critical revision of the manuscript: SS, DK, BL, and NY; generation and provision of resistant and wild type *Plasmodium* strains: PN and SB, obtained funding: SS.

Appendix A. Supplementary data

Supplementary data to this article can be found online at https://doi.org/10.1016/j.ebiom.2019.06.026.

References

[1] Fauci AS, Morens DM. The perpetual challenge of infectious diseases. New Engl J Med 2012 Feb 2;366(5):454–61.
[2] https://www.who.int/malaria/publications/world-malaria-report-2018/report/en/.
[3] Meshnick SR. Artemisinin: mechanisms of action, resistance, and toxicity. Int J Parasitol 2002 Dec 4;32(13):1655–60.
[4] White NJ. Qinghaosu (artemisinin): the price of success. Science 2008 Apr 18;320 (5874):330–4.
[5] White NJ, Pukrittayakamee S, Hien TT, Faiz MA, Mokuolu OA, Dondorp AM. Erratum: malaria The Lancet (2014). Lancet 2014 Jan;383:723–35 (1;383(9918)).
[6] Dondorp AM, Nosten F, Yi P, Das D, Phyo AP, Tarning J, et al. Artemisinin resistance in Plasmodium falciparum malaria. New Engl J Med 2009 Jul 30;361(5):455–67.
[7] Eastman RT, Fidock DA. Artemisinin-based combination therapies: a vital tool in efforts to eliminate malaria. Nat Rev Microbiol 2009 Dec;7(12):864.
[8] Enserink M. Malaria's drug miracle in danger. Science 2010;328:844–6 (PubMed: 20466917).
[9] White NJ. Pharmacokinetic and pharmacodynamic considerations in antimalarial dose optimization. Antimicrob Agents Chemother 2013 Dec 1;57(12):5792–807.
[10] Meshnick SR, Taylor TE, Kamchonwongpaisan S. Artemisinin and the antimalarial endoperoxides: from herbal remedy to targeted chemotherapy. Microbiol Mol Biol Rev 1996 Jun 1;60(2):301–15.
[11] Phyo AP, Nkhoma S, Stepniewska K, Ashley EA, Nair S, McGready R, et al. Emergence of artemisinin-resistant malaria on the western border of Thailand: a longitudinal study. Lancet 2012 May 26;379(9830):1960–6.
[12] Nosten F, White NJ. Artemisinin-based combination treatment of falciparum malaria. Am J Trop Med Hyg 2007 Dec 1;77(6_Suppl):181–92.
[13] Straimer J, Gnädig NF, Witkowski B, Amaratunga C, Duru V, Ramadani AP, et al. K13-propeller mutations confer artemisinin resistance in Plasmodium falciparum clinical isolates. Science 2015 Jan 23;347(6220):428–31.
[14] Dwivedi A, Reynes C, Kuehn A, Roche DB, Khim N, Hebrard M, et al. Functional analysis of Plasmodium falciparum subpopulations associated with artemisinin resistance in Cambodia. Malar J 2017 Dec;16(1):493.
[15] Meshnick SR, Thomas A, Ranz A, Xu CM, Pan HZ. Artemisinin (qinghaosu): the role of intracellular hemin in its mechanism of antimalarial action. Mol Biochem Parasitol 1991 Dec 1;49(2):181–9.
[16] Stocks PA, Bray PG, Barton VE, Al-Helal M, Jones M, Araujo NC, et al. Evidence for a common non-heme chelatable-iron-dependent activation mechanism for semisynthetic and synthetic endoperoxide antimalarial drugs. Angew Chem Int Ed 2007 Aug 20;46(33):6278–83.
[17] Pusic K, Aguilar Z, McLoughlin J, Kobuch S, Xu H, Tsang M, et al. Iron oxide nanoparticles as a clinically acceptable delivery platform for a recombinant blood-stage human malaria vaccine. FASEB J 2013 Mar;27(3):1153–66.
[18] Yuen C, Liu Q. Magnetic field enriched surface enhanced resonance Raman spectroscopy for early malaria diagnosis. J Biomed Opt 2012 Feb;17(1):017005.
[19] Mebrahtu T, Stoltzfus RJ, Chwaya HM, Jape JK, Savioli L, Montresor A, et al. Low-dose daily iron supplementation for 12 months does not increase the prevalence of malaria infection or density of parasites in young Zanzibari children. J Nutr 2004 Nov 1;134(11):3037–41.
[20] Nwanyanwu OC, Ziba C, Kazembe PN, Gamadzi G, Gondwe J, Redd SC. The effect of oral iron therapy during treatment for Plasmodium falciparum malaria with sulphadoxine-pyrimethamine on Malawian children under 5 years of age. Ann Trop Med Parasitol 1996 Jan 1;90(6):589–95.
[21] Verhoef H, West CE, Nzyuko SM, de Vogel S, van der Valk R, Wanga MA, et al. Intermittent administration of iron and sulfadoxine-pyrimethamine to control anemia in Kenyan children: a randomized controlled trial. Lancet 2002 Sep 21;360(9337): 908–14.
[22] Sazawal S, Black RE, Ramsan M, Chwaya HM, Stoltzfus RJ, Dutta A, et al. Effects of routine prophylactic supplementation with iron and folic acid on admission to hospital and mortality in preschool children in a high malaria transmission setting: a community-based, randomized, placebo-controlled trial. Lancet 2006 Jan 14;367 (9505):133–43.
[23] Scholl PF, Tripathi AK, Sullivan DJ. Bioavailable iron and heme metabolism in Plasmodium falciparum. In malaria: drugs, disease and post-genomic biology. Berlin, Heidelberg: Springer; 2005; 293–324.
[24] Subramanian S, Hardt M, Choe Y, Niles RK, Johansen EB, Legac J, et al. Hemoglobin cleavage site-specificity of the Plasmodium falciparum cysteine proteases falcipain-2 and falcipain-3. PLoS One 2009 Apr 9;4(4):e5156.
[25] Roy CN. An update on iron homeostasis: make new friends, but keep the old. Am J Med Sci 2013 Nov 1;346(5):413–9.
[26] Clark MA, Goheen MM, Cerami C. Influence of host iron status on Plasmodium falciparum infection. Front Pharmacol 2014 May 6;5:84.
[27] Bachmann MF, Jennings GT. Vaccine delivery: a matter of size, geometry, kinetics, and molecular patterns. Nat Rev Immunol 2010 Nov;10(11):787.

[28] Lu M, Cohen MH, Rieves D. Pazdur R. FDA report: ferumoxytol for intravenous iron therapy in adult patients with chronic kidney disease. Am J Hematol 2010 May;85 (5):315–9.
[29] Thu MS, Bryant LH, Coppola T, Jordan EK, Budde MD, Lewis BK, et al. Self-assembling nanocomplexes by combining ferumoxytol, heparin, and protamine for cell tracking by magnetic resonance imaging. Nat Med 2012 Mar;18(3):463.
[30] Kandasamy G, Surendran S, Chakrabarty A, Kale SN, Maity D. Facile synthesis of novel hydrophilic and carboxyl-amine functionalized superparamagnetic iron oxide nanoparticles for biomedical applications. RSC Adv 2016;6(102):99948–59.
[31] Trager W, Jensen JB. Human malaria parasites in continuous culture. Science 1976 Aug 20;193(4254):673–5.
[32] Witkowski B, Amaratunga C, Khim N, Sreng S, Chim P, Kim S, et al. Novel phenotypic assays for the detection of artemisinin-resistant Plasmodium falciparum malaria in Cambodia: in-vitro and ex-vivo drug-response studies. Lancet Infect Dis 2013 Dec 1;13(12):1043–9.
[33] Worldwide Antimalarial Resistance Network. Standard Operating Procedure Ring Stage Survival Assays. 11 September 2013. http://www.wwarn.org/sites/default/files/INV10-Standard-Operating-Procedure-Ring-Stage-Survival-Assays.pdf.
[34] Mbengue A, Bhattacharjee S, Pandharkar T, Liu H, Estiu G, Stahelin RV, et al. A molecular mechanism of artemisinin resistance in Plasmodium falciparum malaria. Nature 2015 Apr;520(7549):7683.
[35] Gopalakrishnan AM, Kumar N. Opposing roles for two molecular forms of replication protein a in rad51-Rad54-mediated DNA recombination in Plasmodium falciparum. MBio 2013 Jul 1;4(3) (e00252–13).
[36] Levine RL, Garland D, Oliver CN, Amici A, Climent I, Lenz AG, et al. [49] determination of carbonyl content in oxidatively modified proteins. Methods in Enzymology. Academic Press; 1990 Jan 1. p. 464–78.
[37] Mesquita CS, Oliveira R, Bento F, Geraldo D, Rodrigues JV, Marcos JC. Simplified 2, 4-dinitrophenylhydrazine spectrophotometric assay for quantification of carbonyls in oxidized proteins. Anal Biochem 2014 Aug 1;458:69–71.
[38] Clemmer L, Martins YC, Zanini GM, Frangos JA, Carvalho LJ. Artemether and artesunate show the highest efficacies in rescuing mice with late-stage cerebral malaria and rapidly decrease leukocyte accumulation in the brain. Antimicrob Agents Chemother 2011 Apr 1;55(4):1383–90.
[39] Phenrat T, Liu Y, Tilton RD, Lowry GV. Adsorbed polyelectrolyte coatings decrease Fe0 nanoparticle reactivity with TCE in water: conceptual model and mechanisms. Environ Sci Technol 2009 Jan 29;43(5):1507–14.
[40] Monisha M, Yadav N, Srivastava SB, Singh SP, Lochab B. Sustainable one-step strategy towards low temperature curable superparamagnetic composite based on smartly designed iron nanoparticles and cardanol benzoxazine. J Mater Chem A 2018;6(6):2555–67.
[41] Haynes RK, Chan WC, Lung CM, Uhlemann AC, Eckstein U, Taramelli D, et al. The Fe2+−mediated decomposition, PfATP6 binding, and antimalarial activities of artemisone and other artemisinins: the unlikelihood of C-centered radicals as bioactive intermediates. Chem Med Chem 2007 Oct 8;2(10):1480–97.
[42] Gopalakrishnan AM, Kumar N. Antimalarial action of artesunate involves DNA damage mediated by reactive oxygen species. Antimicrob Agents Chemother 2015 Jan 1; 59(1):317–25.
[43] Li G, Guo X, Arnold K, Jian H, Fu L. Randomised comparative study of mefloquine, qinghaosu, and pyrimethamine-sulfadoxine in patients with falciparum malaria. Lancet 1984 Dec 15;324(8416):1360–1.
[44] Cumming JN, Ploypradith P, Posner GH. Antimalarial activity of artemisinin (qinghaosu) and related trioxanes: Mechanism (s) of action. InAdvances in pharmacology. Academic Press; 1996 Jan 1. p. 253–97.
[45] Törnvall U. Pinpointing oxidative modifications in proteins—recent advances in analytical methods. Anal Methods 2010;2(11):1638–50.
[46] Romero MR, Efferth T, Serrano MA, Castaño B, Macias RI, Briz O, et al. Effect of artemisinin/artesunate as inhibitors of hepatitis B virus production in an "in vitro" replicative system. Antiviral Res 2005 Nov 1;68(2):75–83.
[47] Utzinger J, Shuhua X, N'Goran EK, Bergquist R, Tanner M. The potential of artemether for the control of schistosomiasis. Int J Parasitol 2001 Dec 1;31(14):1549–62.
[48] Efferth T, Dunstan H, Sauerbrey A, Miyachi H, Chitambar CR. The anti-malarial artesunate is also active against cancer. Int J Oncol 2001 Apr 1;18(4):767–73.
[49] Lai H, Singh NP. Oral artemisinin prevents and delays the development of 7, 12-dimethylbenz [a] anthracene (DMBA)-induced breast cancer in the rat. Cancer Lett 2006 Jan 8;231(1):43–8.
[50] Chen Y, Lin X, Park H, Greever R. Study of artemisinin nanocapsules as anticancer drug delivery systems. Nanomedicine 2009 Sep 1;5(3):316–22.
[51] Isacchi B, Arrigucci S, Marca GL, Bergonzi MC, Vannucchi MG, Novelli A, et al. Conventional and long-circulating liposomes of artemisinin: preparation, characterization, and pharmacokinetic profile in mice. J Liposome Res 2011 Sep 1;21(3):237–44.
[52] Wong JW, Yuen KH. Inclusion complexation of artemisinin with α-, β-, and γ-cyclodextrins. Drug Dev Ind Pharm 2003 Jan 1;29(9):1035–44.
[53] Singh NP, Lai HC. Artemisinin induces apoptosis in human cancer cells. Anticancer Res 2004 Jul 1;24(4):2277–80.
[54] Klonis N, Crespo-Ortiz MP, Bottova I, Abu-Bakar N, Kenny S, Rosenthal PJ, et al. Artemisinin activity against Plasmodium falciparum requires hemoglobin uptake and digestion. Proc Natl Acad Sci 2011 Jul 12;108(28):11405–10.
[55] Zanganeh S, Hutter G, Spitler R, Lenkov O, Mahmoudi M, Shaw A, et al. Iron oxide nanoparticles inhibit tumor growth by inducing pro-inflammatory macrophage polarization in tumor tissues. Nat Nanotechnol 2016 Nov;11(11):986.
[56] Hoshyar N, Gray S, Han H, Bao G. The effect of nanoparticle size on in vivo pharmacokinetics and cellular interaction. Nanomedicine 2016 Mar;11(6):673–92.
[57] Goodyer ID, Pouvelle B, Schneider TG, Trelka DP, Taraschi TF. Characterization of macromolecular transport pathways in malaria-infected erythrocytes. Mol Biochem Parasitol 1997 Jul 1;87(1):13–28.

[58] Olliaro PL, Goldberg DE. The plasmodium digestive vacuole: metabolic headquarters and choice drug target. Parasitol Today 1995 Aug 1;11(8):294–7.

[59] Radfar A, Diez A, Bautista JM. Chloroquine mediates specific proteome oxidative damage across the erythrocytic cycle of resistant plasmodium falciparum. Free Radic Biol Med 2008 Jun 15;44(12):2034–42.

[60] Wang J, Zhang CJ, Chia WN, Loh CC, Li Z, Lee YM, et al. Haem-activated promiscuous targeting of artemisinin in Plasmodium falciparum. Nat Commun 2015 Dec 22; 6:10111.

[61] Ismail HM, Barton VE, Panchana M, Charoensutthivarakul S, Biagini GA, Ward SA, et al. A click chemistry-based proteomic approach reveals that 1, 2, 4-Trioxolane and artemisinin antimalarials share a common protein alkylation profile. Angew Chem Int Ed 2016 May 23;55(22):6401–5.